

AD-A107 571

NORTH CAROLINA UNIV AT CHAPEL HILL
COASTAL-TRAPPED AND FRONTAL-TRAPPED WAVES IN A CONTINUOUSLY STR--ETC(U)
AUG 80 M E LUTHER, J M BANE

F/6 8/3

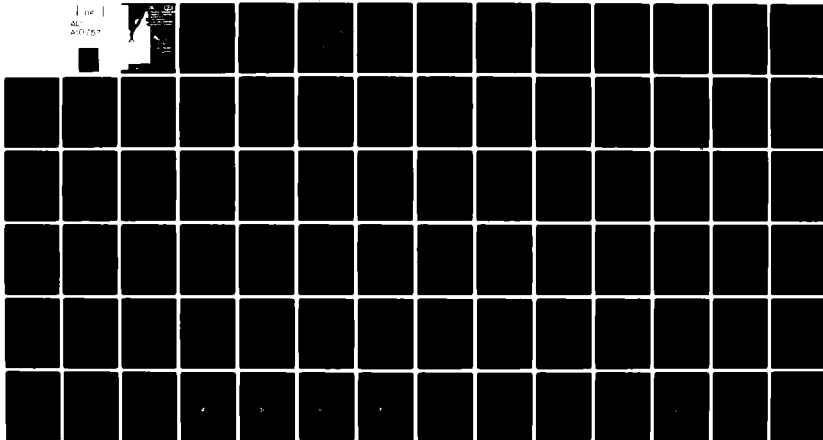
N00014-77-C-0354

UNCLASSIFIED

CMS-81-1

NL

1 of 1
AL
20/75



END
DATE
FILMED
1-82
DTIC

LEVEL II

AD A107571

COASTAL-TROUGH
FRONTAL-TRENCH
WAVES IN A
CONTINUOUSLY
STRATIFIED WESTERN
BOUNDARY CURRENT

A Contribution to the Gulf
Stream Meanders
Experiment

by

Mark E. Lofgren

and

John M. Rienecker

LIBRARY
COLLECTED
NOV 19 1981
H

NAVY
RESEARCH
DEVELOPMENT
AND
TESTING
CENTER

The University of
at Chapel Hill

Technical Report Number

The Ruth H. Hooker Technical Library

NOV 04 1980

Naval Research Laboratory

August 1980

81 11 13 101

TOP FILE

2

UNCLASSIFIED

SECURITY CLASSIFICATION OF THIS PAGE (When Data Entered)

AD-A107571
14
10

REPORT DOCUMENTATION PAGE		READ INSTRUCTIONS BEFORE COMPLETING FORM
1. REPORT NUMBER CMS-80-1	2. GOVT ACCESSION NO. AD-A107571	3. RECIPIENT'S CATALOG NUMBER 4
4. TITLE (and Subtitle) Coastal-Trapped and Frontal-Trapped Waves in a Continuously Stratified Western Boundary Current - A Contribution to the Gulf Stream Meanders Experiment		5. TYPE OF REPORT & PERIOD COVERED Technical report
		6. PERFORMING ORG. REPORT NUMBER CMS-80-1
7. AUTHOR(s) Mark E. Luther and John M. Bane, Jr		8. CONTRACT OR GRANT NUMBER(s) N00014-77-C-0354
9. PERFORMING ORGANIZATION NAME AND ADDRESS University of North Carolina Chapel Hill, NC 27514		10. PROGRAM ELEMENT, PROJECT, TASK AREA & WORK UNIT NUMBERS 17 61155N, RR 031-03-01
11. CONTROLLING OFFICE NAME AND ADDRESS Environmental Sciences Directorate Office of Naval Research Arlington, VA 22217		12. REPORT DATE August 1980
		13. NUMBER OF PAGES 77
14. MONITORING AGENCY NAME & ADDRESS (if different from Controlling Office) UNCLASSIFIED		15. SECURITY CLASS. (of this report) UNCLASSIFIED
16. DISTRIBUTION STATEMENT (of this Report) 12/85		
17. DISTRIBUTION STATEMENT (of the abstract entered in Block 20, if different from Report)		
18. SUPPLEMENTARY NOTES		
19. KEY WORDS (Continue on reverse side if necessary and identify by block number) Coastal-Trapped Frontal-Trapped Waves Gulf Stream Fluctuations		
20. ABSTRACT (Continue on reverse side if necessary and identify by block number) The effects of a realistic western boundary current on the alongshore propagation of sub-inertial waves trapped by a sloping bottom topography are studied using a numerical model incorporating realistic bottom topography and a current field which is in thermal wind balance with the density field. This models the Gulf Stream as it flows along the continental slope off North Carolina. The mean state velocity and density fields do not vary alongshore and are continuous in the horizontal as well as the vertical. The linearized, inviscid equations of motion for small amplitude disturbances yield a single governing equation for		

DD FORM 1473 1 JAN 73

EDITION OF 1 NOV 65 IS OBSOLETE
S/N 0102-LF-014-6601

UNCLASSIFIED 259500
SECURITY CLASSIFICATION OF THIS PAGE (When Data Entered)

the perturbation pressure. This equation is solved using a marching method for elliptical problems. The dispersion relations are obtained by searching for the resonance response of the system to an arbitrary uniform forcing term. Four discrete stable modes of Rossby-like waves are identified, all propagating in the upstream direction. A mode-coupling resonance is found between the first two modes. For small wavenumber, the first mode is trapped within the frontal zone on the cyclonic side of the mean current with a smaller barotropic component over the shelf. This "frontal trapping" is due to the quasi-geostrophic potential vorticity gradient in the mean current. For large wavenumber the first mode becomes primarily a barotropic shelf wave. The second mode is a purely barotropic shelf wave for small wavenumbers, but becomes a frontal-trapped wave at large wavenumbers. For the higher wave modes, most of the energy is trapped near the surface in the frontal zone.

A

R

COASTAL-TRAPPED AND FRONTAL-TRAPPED WAVES
IN A CONTINUOUSLY STRATIFIED
WESTERN BOUNDARY CURRENT

by
Mark E. Luther
and
John M. Bane, Jr.

SDTIC
ELECTE
NOV 19 1981
H

Curriculum in Marine Sciences
University of North Carolina
Chapel Hill, North Carolina 27514

~~APPROVED FOR PUBLIC RELEASE~~
DISTRIBUTION UNLIMITED

Technical Report
Number CMS-80-1

August 1980

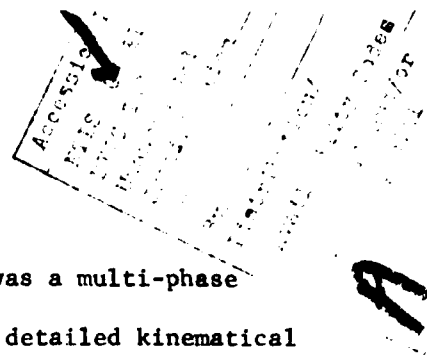
ONR Contract N00014-77-C-0354
NSF Grant OCE-7923413

Copyright by
Mark Edward Luther
All rights reserved
1980

Foreward

The Gulf Stream Meanders Experiment (GSME) was a multi-phase research program with the objective of obtaining detailed kinematical and dynamical descriptions of the mesoscale Gulf Stream meanders which occur along the continental margin of the southeastern United States. The research program was composed of a theoretical component, which began in early 1977, and an observational component, which provided intensive and extensive views of the currents in, and the hydrographic structure of the Gulf Stream between Charleston, South Carolina, and Cape Hatteras, North Carolina, during 1979.

The present Technical Report describes a theoretical study of sub-inertial Gulf Stream fluctuations. This was one contribution to the theoretical component of the GSME. This study was undertaken to provide a basic description of the structure and dispersion properties of stable, Rossby-like waves propagating in a baroclinic, laterally-sheared western boundary current. With a continuously stratified mean flow and variable bottom topography, this model represents a significant step towards realism in the theory of oceanic long wave motions along a continental margin. The results of this study indicate the importance of the interplay among the density field, bottom topography and mean current in determining the normal modes that may propagate in the Gulf Stream. Taken together with field observations made in the GSME, the theoretical results suggest that the strongly sheared, cyclonic Gulf Stream frontal zone is at the heart of mesoscale Gulf Stream variability. Theoretical studies of spatially growing unstable wave motions in a baroclinic Gulf Stream are presently underway at The University of North Carolina to broaden our understanding of the complex dynamical nature of Gulf Stream meanders.



Abstract

The effects of a realistic western boundary current on the alongshore propagation of sub-inertial waves trapped by a sloping bottom topography are studied using a numerical model incorporating realistic bottom topography and a current field which is in thermal wind balance with the density field. This models the Gulf Stream as it flows along the continental slope off North Carolina. The mean state velocity and density fields do not vary alongshore and are continuous in the horizontal as well as the vertical. The linearized, inviscid equations of motion for small amplitude disturbances yield a single governing equation for the perturbation pressure. This equation is solved using a marching method for elliptic problems. The dispersion relations are obtained by searching for the resonance response of the system to an arbitrary uniform forcing term. Four discrete stable modes of Rossby-like waves are identified, all propagating in the upstream direction. A mode-coupling resonance is found between the first two modes. For small wavenumber, the first mode is trapped within the frontal zone on the cyclonic side of the mean current with a smaller barotropic component over the shelf. This "frontal trapping" is due to the quasi-geostrophic potential vorticity gradient in the mean current. For large wavenumber, the first mode becomes primarily a barotropic shelf wave. The second mode is a purely barotropic shelf wave for small wavenumbers, but becomes a frontal-trapped wave at large wavenumbers. For the higher wave modes, most of the energy is trapped near the surface in the frontal zone.

<u>Table of Contents</u>	<u>Page</u>
1. Introduction	1
2. Formulation of Governing Equations	9
3. Description of Model Geometry	17
4. Method of Solution	20
5. Results	23
6. Discussion	28
7. Conclusions	32
Acknowledgments	34
Appendix	
A1. Separation of time dependent flow from mean flow	35
A2. Formulation of governing equation	39
A3. Finite difference form of the forced equation	42
A4. Subroutine EVP9G	45
References	49
Legend of Figures	52
Illustrations	55

1. Introduction

Much research in physical oceanography during the past few years has been devoted to the subject of coastal-trapped waves. This general classification of sub-inertial frequency, topographically trapped waves can be broken down into several subclassifications under certain limiting conditions (Wang and Mooers, 1976).

In the simple case of an ocean of constant depth with a vertical wall at the coast, these waves are coastal Kelvin waves. In a homogeneous ocean over a constantly sloping bottom topography, the general coastal-trapped wave reduces to the quasi-geostrophic edge wave (Reid, 1958). If the slope of the bottom topography changes away from the coast, such as a finite width continental shelf adjoining a constant depth deep sea region, the familiar barotropic continental shelf wave results (Robinson, 1964; Mysak, 1967; Buchwald and Adams, 1968).

The structure of the coastal-trapped wave becomes more complicated in the presence of a laterally sheared barotropic mean current (Niiler and Mysak, 1971; Grimshaw, 1976; Brooks and Mooers, 1977a,b) or in the presence of a level stratification over a sloping bottom topography (Allen, 1975; Wang, 1975; Wang and Mooers, 1976; Clarke, 1977; Huthnance 1978). Mysak (1980) presents a comprehensive review of the theory of coastal-trapped waves.

This study extends the present theory to include the effects of a continuously stratified, laterally and vertically sheared western boundary current flowing along the continental slope.

Reid (1958) first described quasi-geostrophic edge waves trapped over a constantly sloping continental shelf of infinite extent. These low frequency waves are supported by the potential vorticity gradient

associated with the sloping bottom. They are right bounded, that is, they propagate their phase with the shallow water to their right, in the northern hemisphere. Reid called these waves "quasi-geostrophic" because the balance in the momentum equations was essentially geostrophic.

Continental shelf waves were first observed by Hamon (1962) as non-barometric sea level disturbances that propagated northward along the Australian coast from Sidney to Coff's Harbor. Robinson (1964) developed a simple linear theory to explain Hamon's observations. Robinson's model incorporated a constantly sloping continental shelf of finite width adjoining a constant depth deep sea region. He called these low-frequency, vorticity wave motions continental shelf waves because they were trapped over the shelf by the sloping bottom and decayed exponentially away from the shelf.

Mysak (1967, 1968) showed that Reid's quasi-geostrophic edge waves and Robinson's continental shelf waves were closely related. Both waves are special cases of a topographic Rossby wave. At short wavelengths, the shelf waves become quasi-geostrophic waves, since they are trapped more closely to the coast and cannot "see" the edge of the shelf. Mysak (1967) considered the effects of atmospheric pressure variations on the generation of shelf waves. He also included a simple stratification and current in the deep sea region of Robinson's (1964) model geometry.

Buchwald and Adams (1968) extended these linear theories to include a more realistic bottom topography. Using an exponential shelf and slope depth profile, they showed that the offshore trapping scale for the shelf wave modes was the shelf width. Adams and Buchwald (1969) in the same model geometry, showed that wind stress, rather than

atmospheric pressure, was responsible for the generation of shelf waves. Gill and Schumann (1974) gave a more detailed analysis of this generating mechanism. They showed that the alongshore component of the wind drove an Ekman transport in the surface mixed layer. Since shelf waves are non-divergent, conservation of mass requires that there is a return flow through the interior. It is this return flow over the strongly sloping bottom that changes the vorticity by vortex stretching, and hence generates shelf waves.

Recent theoretical studies have shown that lateral boundary current shear strongly affects the propagation of barotropic shelf waves. In areas such as the Gulf Stream off the east coast of the United States, the horizontal shear of the mean current can be comparable to the Coriolis parameter f . Shelf waves can be significantly advected by the mean current and have their propagation characteristics strongly modified. They can extract energy from the mean current through the process of barotropic instability. The strong shear of the current can support a new class of shear waves. Niiler and Mysak (1971) examined the trapped wave solutions for the case of a constantly sloping shelf of finite width with a V-shaped alongshore mean current. This topography and current structure was chosen to model the Gulf Stream as it flows along the southeastern coast of the United States. They found that the direction of shelf wave propagation was reversed by the mean flow at a high wave number cut-off. There also exists a class of shear waves that always travel in the downstream direction. The dispersion curves for the shelf wave and the shear wave cross in a particular range of wavenumber, where the waves become unstable. At wavenumbers above this range, the two dispersion curves change families, the

shelf wave curve becoming a shear wave, and the shear wave curve becoming a shelf wave.

Brooks and Mooers (1977b) studied stable barotropic shelf waves over an exponential depth profile with an exponential alongshore mean current. They also found that the direction of shelf wave propagation was reversed by the mean flow at a high wavenumber cut-off. Brooks (1975), Grimshaw (1976) and McKee (1977) discussed the problem of critical layers in the mean flow; that is, a level in the mean flow where the wave phase speed equals the mean current velocity. In addition to the discrete spectrum of shelf wave modes, there is a continuum of allowable critical layer solutions in the dispersion plane, with phase speeds lying in the range of the current speed.

All of the shelf wave models discussed above have dealt with a homogenous ocean. The presence of stratification can alter the properties of shelf waves and also can allow other types of waves to exist. A number of models have incorporated a level stratification in the study of coastal-trapped waves.

Mysak (1967) and Gill and Clarke (1974) examined long waves in a two-layer ocean with only the top layer extending over the shelf. It was shown by Allen (1975) and Wang (1975) that the barotropic and baroclinic modes were coupled when the two-layer stratification extended over a sloping continental shelf. Allen (1975) showed that the strength of this coupling depended on the ratio of the internal radius of deformation to the length scale of the topographic variation. Both Allen (1975) and Wang (1975) found that where the dispersion curves of the shelf waves and the single Kelvin wave appeared to cross, there was actually a change of modal structure of the waves. Wang (1975) called this

coupling between the shelf waves and the internal Kelvin wave a "resonance coupling". This terminology was introduced by Eckart (1962) in a study of internal waves.

Wang and Mooers (1976) also found this resonance phenomenon in a continuously stratified model. They found that in the limit of a vanishing coastal wall, topographic Rossby waves were the only class of sub-inertial frequency, coastal-trapped wave motion. The topographic Rossby wave reduces to a barotropic continental shelf wave in the special case of small stratification, and to a bottom-trapped wave (Rhines, 1970) in the special case of large stratification. Huthnance (1978) showed analytically that for a monotonically increasing depth profile with a level density stratification there was only one infinite discrete set of trapped sub-inertial modes with frequency decreasing as mode number increased. Clarke (1977) showed that in the long wave limit, these waves were a hybrid between shelf waves and internal Kelvin waves. These models, however, have not considered the presence of sloping isopycnals with an associated vertically sheared mean current in thermal wind balance with the mean density field.

The Gulf Stream region off the southeastern coast of the United States is characterized by the presence of strongly sloping density surfaces combined with strong lateral and vertical current shear. Orlandi (1969), using a two-layer model, and Orlandi and Cox (1973), using a continuous stratification, studied baroclinically unstable waves in a western boundary current, but neglected stable waves.

Bane and Hsueh (1980) investigated the role of a density front in determining the dispersion characteristics of stable topographic Rossby waves. They found a "complementary mode" in which a barotropic wave

over the shelf matched with a baroclinic wave at the density front. Bane (1980) developed a two-layer model which incorporates a general continental shelf and slope topography with a thermal-wind mean current in the upper layer. He identified four types of stable, sub-inertial frequency, Rossby-like waves. They are the barotropic shelf wave, the quasi-geostrophic edge wave, the complementary mode edge wave, and a new frontal-trapped wave, so-called because its amplitude is trapped within the frontal zone on the cyclonic side of the mean current. The dispersion curves for this model exhibit the mode-coupling resonance phenomenon, allowing the characteristics of the component waves to be interchanged along a composite dispersion curve. An obvious limiting feature of these two-layer models is that they lack sufficient vertical resolution.

There is a great deal of evidence to support the existence of shelf waves in general (Hamon, 1962, 1966; Mooers and Smith, 1968; Cartwright, 1969; Cutchin and Smith, 1973) and particularly off the coast of North Carolina (Mysak and Hamon, 1969; Brooks, 1978). It has been suggested that meanderings of the Gulf Stream in this area may be related to coastal-trapped waves (Brooks, 1978; Brooks and Bane, 1978; Bane and Brooks, 1979a). Stable, propagating, wave-like meander patterns in the inshore edge of the Gulf Stream have been observed to be a dominant mode of oscillation of the Stream (Legeckis, 1979). The existing theoretical models, however, have not dealt adequately with the complex dynamics found in this region. On the inshore, or cyclonic, side of the Gulf Stream, both the strongly sloping density surfaces and the large horizontal shear of the mean flow contribute in the same sense as the sloping bottom to the ambient potential vorticity gradient, giving

rise to dual trapping mechanisms. This second trapping mechanism is the gradient of the quasi-geostrophic potential vorticity (cf., Pedlosky, 1979). It is the two-layer analogue of the quasi-geostrophic potential vorticity gradient that supports the frontal trapped waves described by Bane (1980). The maximum velocity of the Stream is on the same order as the phase speed of topographic Rossby waves, but in the opposite direction, so that one would expect significant advection of the waves. It has been shown that when both stratification and topography are present, the barotropic and baroclinic modes are coupled (Allen, 1975). Thus, the presence of a western boundary current in a coastal-trapped wave model can alter the properties of the coastal-trapped wave modes, and can allow the existence of a new class of frontal-trapped waves. Moreover, one expects the coastal-trapped waves to be coupled with the frontal-trapped waves due to the stratification. To aid in the study of these effects, the present model includes a realistic western boundary current flowing along a continental slope.

Mysak (1980) points out that the presence of a wide flat shelf, as is found off the coast of the Carolinas, enhances the mode-coupling resonance found by Wang and Mooers (1976). Bane (1980) suggests that this is due to changes in the dispersion properties of the different component waves with changing shelf width. This model simulates the Gulf Stream as it flows along the continental slope off Onslow Bay, North Carolina, where the shelf is very wide. In this continuous stratification model, the different wave types found in Bane's (1980) two-layer model are more subtly coupled and are more difficult to distinguish; however, the frontal-trapped wave is clearly present. A hybrid between a topographic Rossby-like wave and a frontal-trapped wave is found also.

The next section describes the formulation of the governing equation and the boundary conditions. Section 3 describes the mean state for the model, and section 4 outlines the numerical solution scheme. The results of the computations are presented in section 5, and are discussed in section 6. The conclusions are summarized in section 7.

2. Formulation

Consider a model eastern continental shelf and slope region with a steady alongshore flow in geostrophic and hydrostatic balance with the density field. A straight coastline is assumed along the y-axis, with the x-axis pointing offshore and the z-axis pointing vertically upward. The depth, $h(x)$, is a monotonically increasing function of x only. A schematic of this idealized geometry is shown in Fig. 2.1. The fluid is assumed to be inviscid, incompressible, non-diffusive, and continuously density-stratified. Variations in the Coriolis parameter, f , are neglected. The equations of motion for small amplitude disturbances are

$$\rho \left[\frac{Du}{Dt} - fv \right] = -p_x$$

$$\rho \left[\frac{Dv}{Dt} + fu \right] = -p_y$$

$$\rho \frac{Dw}{Dt} = -p_z - \rho g$$

$$u_x + v_y + w_z = 0$$

$$\frac{D\rho}{Dt} = 0$$

where subscripts denote differentiation, and

$$\frac{D}{Dt} = \frac{\partial}{\partial t} + u \frac{\partial}{\partial x} + v \frac{\partial}{\partial y} + w \frac{\partial}{\partial z} .$$

Following the notation of Mooers (1975a,b), the dependent variables are separated into mean and fluctuating components (denoted by overbars and primes, respectively):

$$v = \bar{v} + v' , \quad u = u' , \quad w = w' ,$$

$$\rho = \rho_0 + \bar{\rho} + \rho' ,$$

$$p = p_0 + \bar{p} + p' ,$$

$$\text{where } p_0 = -\rho_0 g z$$

$$\text{and } (\bar{\rho}, \rho') \ll \rho_0 .$$

The buoyancy and the nonhydrostatic pressure are defined as

$$b = -\frac{g\rho}{\rho_0} = b_0 + \bar{b} + b' ,$$

$$\pi = \frac{p - p_0}{\rho_0} = \bar{\pi} + \pi' .$$

The equations of motion are time averaged and the wave motion is separated from the mean flow (see Appendix A1). Reynolds stresses and non-linear or wave-wave interaction terms are neglected and a Boussinesq approximation is adopted.

The mean flow is governed by

$$f\bar{v} = \bar{\pi}_x \tag{2.1}$$

$$0 = -\bar{\pi}_z + \bar{b} \tag{2.2}$$

Together, (2.1) and (2.2) yield the thermal wind relation

$$f\bar{v}_z = M^2$$

where $M^2 = \bar{h}_x$ is the horizontal analogue to the Brunt-Vaisala frequency,

$$N^2 = \frac{-g\bar{\rho}_z}{\rho_0} = \bar{h}_z .$$

A hydrostatic balance is assumed, since only sub-inertial frequency motions are being considered. The wave motion, without the primes, is governed by

$$u_t + \bar{v}u_y - fv = -\pi_x \quad (2.3)$$

$$v_t + \bar{v}v_y + (f + \bar{v}_x)u + \bar{v}_z w = -\pi_y \quad (2.4)$$

$$0 = -\pi_z + b \quad (2.5)$$

$$u_x + v_y + w_z = 0 \quad (2.6)$$

$$b_t + \bar{v}b_y + M^2 u + N^2 w = 0 \quad (2.7)$$

Because of the strong horizontal density gradients, M^2 must be included in (2.7); therefore, from the thermal wind relation, \bar{v}_z must be retained in (2.4). The strong lateral shear of the Gulf Stream, which augments the background potential vorticity of the region, requires the inclusion of \bar{v}_x in (2.4).

Only alongshore propagating disturbances are considered; therefore, all perturbation variables (u, v, w, π, b) are assumed to take the form $e^{i(\sigma_0 t + \ell y)}$ for their (y, t) dependence, where σ_0 is the wave frequency, ℓ is the alongshore wavenumber, and $i = (-1)^{1/2}$. Differentiation with respect to t and y thus becomes equivalent to multiplication by $i\sigma$ and $i\ell$, respectively. The intrinsic frequency is the frequency seen by a fluid particle at a particular x and z , and is defined as $\sigma(x, z) = \sigma_0 + \bar{v}(x, z)\ell$. The mean current, \bar{v} , is always positive (a northward flowing current), so that for a wave propagating in the

positive y (downstream) direction (either σ_0 or ℓ negative, but not both), there exists the possibility of a critical surface where $\sigma(x,z) = 0$, i.e., the wave phase is propagating at the same speed as the local medium. For this study, only stable waves propagating in the negative y (upstream) direction will be considered, so that σ_0 and ℓ are always positive, and critical levels are avoided. Equations (2.3) through (2.7) now become

$$i\sigma u - fv = -\pi_x \quad (2.8)$$

$$i\sigma v + (f + \bar{v}_x)u + v_z w = -i\ell\pi \quad (2.9)$$

$$0 = -\pi_z + b \quad (2.10)$$

$$u_x + i\ell v + w_z = 0 \quad (2.11)$$

$$i\sigma b + M^2 u + N^2 w = 0 \quad (2.12)$$

Eliminating the buoyancy, b , between (2.10) and (2.12), then solving (2.8) through (2.10) for u , v and w in terms of π , gives

$$u = \frac{i}{\Delta} \left(-\sigma N^2 \pi_x + \sigma M^2 \pi_z - \ell f N^2 \pi \right) \quad (2.13)$$

$$v = \frac{1}{f\Delta} \left[\left(N^2 \sigma_f^2 - M^4 \right) \pi_x - \sigma^2 M^2 \pi_z + \sigma f \ell N^2 \pi \right] \quad (2.14)$$

$$w = \frac{i}{\Delta} \left[\sigma M^2 \pi_x - \sigma \left(\sigma_f^2 - \sigma^2 \right) \pi_z + \ell f M^2 \pi \right] \quad (2.15)$$

where $\Delta = N^2 \left(\sigma_f^2 - \sigma^2 \right) - M^4$, and $\sigma_f^2 = f(f + \bar{v}_x)$ is the square of the effective local inertial frequency (Mooers, 1975a). Substituting (2.13) through (2.15) into the continuity equation (2.11) and applying the thermal wind relation yields the governing equation for the perturbation pressure, π :

$$\begin{aligned}
\pi_{xx} - 2 \frac{M^2}{N^2} \pi_{xz} + \frac{(\sigma_f^2 - \sigma^2)}{N^2} \pi_{zz} + \frac{1}{\Delta} \left[\frac{M^2}{N^2} \frac{\partial \Delta}{\partial z} - \frac{\partial \Delta}{\partial x} \right] \pi_x \\
+ \left[\frac{1}{\Delta} \left\{ \frac{M^2}{N^2} \frac{\partial \Delta}{\partial x} - \frac{(\sigma_f^2 - \sigma^2)}{N^2} \frac{\partial \Delta}{\partial z} \right\} - 2 \frac{\sigma \ell}{f} \frac{M^2}{N^2} \right] \pi_z \\
+ \left[\frac{\ell f}{\sigma \Delta} \left(\frac{M^2}{N^2} \frac{\partial \Delta}{\partial z} - \frac{\partial \Delta}{\partial x} \right) - \ell^2 \right] \pi = 0 . \quad (2.16)
\end{aligned}$$

The boundary conditions chosen for sub-inertial motion are as follows. At the surface ($z = 0$), a rigid lid is imposed, i.e., $w = 0$. The rigid lid approximation suppresses any wave-associated sea level elevations and free surface divergences while retaining the pressure gradients along the surface. This has the effect of filtering out any external gravity waves. Huthnance (1978) showed that the free surface divergence effects were generally very small for sub-inertial waves, and that the eigenfrequencies of these waves were increased only slightly by invoking the rigid lid approximation. Using (2.15), the boundary condition at $z = 0$ becomes

$$M^2 \pi_x - (\sigma_f^2 - \sigma^2) \pi_z + \frac{\ell f}{\sigma} M^2 \pi = 0 \quad \text{at } z=0. \quad (2.17)$$

At $z = -h(x)$, there is no flow normal to the bottom, which implies that $w = -uh_x$, or from (2.13) and (2.15),

$$(M^2 - N^2 h_x) (\pi_x + \frac{\ell f}{\sigma} \pi) + (M^2 h_x - (\sigma_f^2 - \sigma^2)) \pi_z = 0 \quad \text{at } z=-h(x). \quad (2.18)$$

At the coastline, there is no flow normal to shore; that is, at $x = 0$, $u = 0$, or from (2.13)

$$\pi_x - \frac{M^2}{N^2} \pi_z + \frac{\ell f}{\sigma} \pi = 0 \quad \text{at } x=0. \quad (2.19)$$

Trapped wave solutions are sought, requiring that all solutions decay far offshore; that is,

$$\pi \rightarrow 0 \quad \text{as } x \rightarrow \infty. \quad (2.20)$$

Equations (2.16) through (2.20) form an eigenvalue problem in σ_0 and ℓ . In the limiting case of a level stratification and no mean current ($\bar{v} = 0$ and $M^2 = 0$), (2.16) through (2.20) reduce to the equations used by Wang and Mooers (1976) and by Huthnance (1978). Equation (2.16) is elliptic for the values of N^2 , M^2 and \bar{v}_x encountered in a typical western boundary current profile provided $\sigma_0 < f$. It is convenient to solve (2.16) - (2.20) in a rectangular domain; therefore, the independent variables (x, z) are transformed to (x, ζ) , where $\zeta = zH/h(x)$, H being the maximum depth and $h(x)$ the depth at offshore distance x . The governing equation (2.16) then becomes

$$\begin{aligned} \pi_{xx} - \frac{2}{h} \left(h_x \zeta + \frac{M^2}{N^2} H \right) \pi_{x\zeta} + \frac{1}{h^2} \left\{ h_x^2 \zeta^2 + 2 \frac{M^2}{N^2} h_x H \zeta + \frac{\sigma_f^2 - \sigma^2}{N^2} H \right\} \pi_{\zeta\zeta} \\ + \frac{1}{\Delta} \left(\frac{M^2}{N^2} \frac{\partial \Delta}{\partial z} - \frac{\partial \Delta}{\partial x} \right) \pi_x + \frac{1}{h} \left[\left\{ \frac{2}{h} h_x^2 - h_{xx} + \frac{h_x}{\Delta} \left(\frac{\partial \Delta}{\partial x} - \frac{M^2}{N^2} \frac{\partial \Delta}{\partial z} \right) \right\} \zeta \right. \\ \left. + 2 \frac{M^2}{N^2} H \left(\frac{h_x}{h} - \frac{\sigma \ell}{f} \right) + \frac{H}{\Delta} \left\{ \frac{M^2}{N^2} \frac{\partial \Delta}{\partial x} - \frac{(\sigma_f^2 - \sigma^2)}{N^2} \frac{\partial \Delta}{\partial z} \right\} \right] \pi_\zeta \\ + \left\{ \frac{\ell f}{\sigma \Delta} \left(\frac{M^2}{N^2} \frac{\partial \Delta}{\partial z} - \frac{\partial \Delta}{\partial x} \right) - \ell^2 \right\} \pi = 0. \end{aligned} \quad (2.21)$$

The boundary conditions become

$$\pi_x - \zeta \frac{h_x}{h} \pi_\zeta + \frac{\ell f}{\sigma} \pi = 0 \quad \text{at } x = 0; \quad (2.22)$$

$$M^2 \pi_x - \left(\sigma_f^2 - \sigma^2 \right) \frac{H}{h} \pi_\zeta + \frac{M^2 \ell f}{\sigma} \pi = 0 \quad \text{at } \zeta = 0; \quad (2.23)$$

$$\left(\frac{M^2}{N^2} - h_x \right) \pi_x + \frac{H}{h} \left[2 \frac{M^2}{N^2} h_x - h_x^2 - \frac{(\sigma_f^2 - \sigma^2)}{N^2} \right] \pi_\zeta + \frac{\ell f}{\sigma} \left(\frac{M^2}{N^2} - h_x \right) \pi = 0$$

$$\text{at } \zeta = -H. \quad (2.24)$$

The variables are made dimensionless by the relations

$$x^* = x/L, \quad z^* = z/H, \quad \zeta^* = \zeta/H, \quad h^* = h/H, \quad \sigma^* = \sigma/f, \quad \ell^* = \ell/L, \quad \sigma_f^* = \sigma_f/f,$$

$$N^{2*} = N^2/N_{\max}^2, \quad \text{and } M^{2*} = M^2/M_{\max}^2.$$

In dimensionless form, equation (2.21) becomes, with the asterisks dropped,

$$\begin{aligned} \pi_{xx} - \frac{2}{h} \left(h_x \zeta + \alpha \frac{M^2}{N^2} \right) \pi_{x\zeta} + \frac{1}{h^2} \left[h_x^2 \zeta^2 + 2\alpha \frac{M^2}{N^2} h_x \zeta + \frac{(\sigma_f^2 - \sigma^2)}{S^2 N^2} \right] \pi_{\zeta\zeta} \\ + \frac{1}{\Lambda} \left(\alpha \frac{M^2}{N^2} \frac{\partial \Delta}{\partial z} - \frac{\partial \Delta}{\partial x} \right) \pi_x + \frac{1}{h} \left[\left\{ 2 \frac{h_x^2}{h} - h_{xx} + \frac{h_x}{\Delta} \left(\frac{\partial \Delta}{\partial x} - \alpha \frac{M^2}{N^2} \frac{\partial \Delta}{\partial z} \right) \right\} \zeta \right. \\ \left. + \frac{1}{\Lambda} \left(\alpha \frac{M^2}{N^2} \frac{\partial \Delta}{\partial x} - \frac{(\sigma_f^2 - \sigma^2)}{S^2 N^2} \frac{\partial \Delta}{\partial z} \right) + 2\alpha \frac{M^2}{N^2} \left(\frac{h_x}{h} - \sigma \ell \right) \right] \pi_\zeta \\ + \left\{ \frac{\ell}{\sigma \Lambda} \left(\alpha \frac{M^2}{N^2} \frac{\partial \Delta}{\partial x} - \frac{\partial \Delta}{\partial z} \right) - \ell^2 \right\} \pi = 0 \end{aligned} \quad (2.25)$$

with the boundary conditions

$$\pi_x - \frac{\zeta}{h} h_x \pi_\zeta + \frac{\ell}{\sigma} \pi = 0 \quad \text{at } x = 0; \quad (2.26)$$

$$M^2 \pi_x - \frac{f^2 L}{M_{\max}^2 H h} \left(\sigma_f^2 - \sigma^2 \right) \pi_\zeta + \frac{M^2 \ell}{\sigma} \pi = 0 \quad \text{at } \zeta = 0; \quad (2.27)$$

$$\begin{aligned} \left(\alpha \frac{M^2}{N^2} - h_x \right) \pi_x + \frac{1}{h} \left(2\alpha \frac{M^2}{N^2} h_x - h_x^2 - \frac{(\sigma_f^2 - \sigma^2)}{S^2 N^2} \right) \pi_\zeta \\ + \frac{\ell}{\sigma} \left(\alpha \frac{M^2}{N^2} - h_x \right) \pi = 0 \quad \text{at } \zeta = -1; \end{aligned} \quad (2.28)$$

$$\text{and } \pi \rightarrow 0 \quad \text{as } x \rightarrow \infty \quad (2.29)$$

where $\alpha = \frac{M_{\max}^2 L}{N_{\max}^2 H}$ is the "aspect ratio" for the density field

and $S = \frac{N_{\max} H}{fL}$ is a stratification parameter (also called a Burger number), which is the ratio of the internal Rossby radius of deformation

number $r_i = \frac{N_{\max} H}{f}$ to the horizontal length scale L .

3. Description of the Model Geometry

The background mean current in this study reasonably approximates the Gulf Stream as it flows along the coast of North Carolina (Richardson, Schmitz and Niiler, 1969). It is essentially the same as that used by Orlanski and Cox (1973) as their initial conditions. This form is chosen because the values of N^2 , M^2 , \bar{v} and their derivatives are easily evaluated at any point in the solution domain.

The mean velocity, \bar{v} , is assumed to be in geostrophic balance with the density field which is determined entirely by the temperature. The mean velocity is in the positive y (northward) direction, and does not vary with y or t. The analytic expression for the temperature field used by Orlanski and Cox (1973) is

$$T(x,z) = T_0 - \Delta T(3-2(\delta x + 1)e^{-\delta x})(\epsilon z - 1)e^{2\epsilon z} \quad (3.1)$$

where the parameters T_0 , ΔT , δ and ϵ are adjusted to give the desired temperature profile. The density is given by

$$\rho(x,z) = \rho_0(1 - \alpha T(x,z)) \quad (3.2)$$

where α is the thermal expansivity of sea water, and is taken to be a constant. By using (3.1), (3.2) and the thermal wind relation, the expression for the mean velocity is found to be

$$\bar{v}(x,z) = \frac{g\alpha\Delta T}{f\epsilon} \delta^2 x e^{-\delta x} (3/2 - \epsilon z) e^{2\epsilon z}. \quad (3.3)$$

The horizontal shear of the mean velocity is

$$\bar{v}_x(x, z) = \frac{g\alpha\Delta T}{f\epsilon} \delta^2 (1-\delta x) e^{-\delta x} (3/2 - \epsilon z) e^{2\epsilon z} \quad (3.4)$$

From the definitions of Brunt-Vaisala frequency, N^2 , and its horizontal analogue, M^2 , it is found that

$$N^2(x, z) = -g\alpha\Delta T (3 - 2(\delta x + 1)e^{-\delta x}) (2\epsilon z - 1) \epsilon e^{2\epsilon z} \quad (3.5)$$

$$M^2(x, z) = -2g\alpha\Delta T (\delta^2 x e^{-\delta x}) (\epsilon z - 1) e^{2\epsilon z} \quad (3.6)$$

The bottom topography used in the model has a hyperbolic tangent form

$$h(x) = H_{\text{wall}} + \frac{H_0 - H_{\text{wall}}}{2} [1 + \tanh(s(x-a))]$$

where H_{wall} is the depth at the coastline, H_0 is the offshore maximum depth, a is the offshore distance of the maximum slope and s is proportional to the maximum slope.

The parameters T_0 , ΔT , δ , and ϵ for the current and density fields, and a , s , and H_{wall} for the bottom topography, are chosen to model the Gulf Stream as it flows along the continental slope off Onslow Bay, North Carolina, at about 33.5°N latitude (Fig. 3.1). A current section from the area, after Richardson et al. (1969), is shown in Figure 3.2. For the model, the deep water temperature T_0 is chosen to be 4°C . The vertical temperature difference ΔT , is 7°C . To give a current of about

200 km wide, δ , the inverse of the horizontal scale length, is set equal to $3 \times 10^{-5} \text{ m}^{-1}$. The vertical scale of the current is determined by ϵ , which for a 1500m deep current is equal to $1.3 \times 10^{-3} \text{ m}^{-1}$. The in-shore edge of the current, or the front, is placed 100 km from shore, which is just over the shelf break. The position of maximum bottom slope, a , is 145 km from shore and the maximum slope is equal to 0.05 which corresponds to $s = 2.5 \times 10^{-5}$. The resulting velocity and temperature fields are shown in Figures 3.3 and 3.4 respectively. The depth of the coastal wall is 100 m, or 2.5% of the maximum depth $H_0 = 4000\text{m}$. The offshore coordinate is made dimensionless by the width of the current, $L = 200 \text{ km}$, and the vertical coordinate by the maximum depth H_0 . The offshore boundary is imposed at a distance $x = 2L$. It will be seen later that this is sufficiently far offshore, as all solutions die out far inshore of this boundary. The presence of the coastal wall is somewhat unrealistic and is purely for mathematical convenience. If the depth at the coast is allowed to go to zero, some of the coefficients in (2.25) become infinite. The implications of a finite coastal wall will be discussed in a later section.

4. Method of Solution

The governing equation (2.25) is a two dimensional, second order, partial differential equation in a rectangular domain. Solutions to this equation subject to the boundary conditions (2.26) - (2.29) are obtained for a particular σ_0 and ℓ using the marching method for elliptic partial differential equations of Roache (1978). For a fixed ℓ , the eigenvalues of σ_0 are found by searching for the resonance response of the system to a progressive wave forcing term of unit amplitude.

The marching method is "direct"; that is, it produces an algebraically exact answer in a finite number of steps, as opposed to an iterative method in which each iteration gives a better approximation to the exact solution. To solve the boundary value problem for a fixed σ_0 and ℓ , the solution is guessed at one boundary and the finite difference form of the equation is "marched" through to the opposite boundary. The results of the march are then compared to the boundary condition and the initial guess is corrected accordingly. A second march then gives the correct solution. A complete description of the algorithm used can be found in Roache (1978).

The stability of the marching method is highly dependent on the number of grid points in the direction of march, J . The method becomes unstable for large J , primarily due to machine round-off error (see Roache, 1978). This behavior places an upper bound on the resolution of the method. For this problem, suitable results are obtained using 16 grid points in the ζ direction, the direction of march, and 31 points in the x direction (Figure 4.1). The use of a larger value for J results in unacceptable error propagation through the march, even when using double precision on the CRAY1 computer. The grid spacing used gives

dimensionless horizontal and vertical resolutions of 0.0667. In dimensional coordinates, this gives a horizontal resolution of $13 \frac{1}{3}$ km, since the offshore boundary is placed at $x = 2L = 400$ km. The vertical resolution is a function of x , and in dimensional coordinates, $\Delta z = 0.0667 h(x)$.

The dispersion relations are found by repeatedly solving the boundary value problem for different values of σ_0 and ℓ . Dimensionless wavenumber ℓ is set at 40 increments between 0 and 5.0. For each value of ℓ , the boundary value problem is solved for 60 values of σ_0 between 0 and 0.6. The total kinetic energy over the entire solution grid is calculated for each value of σ_0 and stored. The array of kinetic energy values for that particular ℓ is then searched to locate the local maxima. These maxima are considered an indication of a resonance response of the system and therefore the points (σ_0, ℓ) corresponding to these maxima lie on or very near a dispersion curve. Fig. 4.2 shows a plot of integrated kinetic energy versus σ_0 for $\ell = 2.0$. The dispersion relation is obtained by contouring the resonance points. To get sufficient resolution in frequency-wavenumber space requires the solution of the boundary value problem 2400 times. Each solution requires about one second on the CRAY1, so that to produce an entire dispersion relation requires forty minutes of CRAY1 CPU time. For wavenumbers greater than 5.0 the horizontal scales of the motions approach the horizontal resolution of the numerical method; therefore the dispersion relation could not be extended to higher wavenumbers.

This method is tested using the model of Wang and Mooers (1976) for a flat stratification. Using their depth profile

$$h(x) = \begin{cases} 0.005 + 0.36 x , & 0.42 \geq x \geq 0 \\ -0.33 + 1.33 x , & 1.02 \geq x \geq 0.4 \\ 1.0 & , \quad x \geq 1.0 \end{cases}$$

and static stability

$$N^2(z) = -(z - 0.05)/(z - 0.3)^2$$

and a stratification parameter S of order unity, this method reproduces their results (Figure 4.3). Assuming that the results of Wang and Mooers (1976) are correct, it seems safe to assume that this method produces sound results.

5. Results

The dispersion curves obtained for the model are shown in Figure 5.1. Five curves are distinctly identifiable from the eigenvalue search. A mode numbering convention is used to identify the curves in the dispersion diagram. The uppermost curve is called "mode 0", the next highest curve is called "mode 1" and so on. The mode numbers do not imply any particular wave structure. The uppermost curve, mode 0, is an internal Kelvin wave trapped near the bottom against the vertical coastal wall. All of the energy is contained in the alongshore and vertical velocities. This mode is non-dispersive and for wavenumber ℓ greater than 1.0, it is no longer in the range of sub-inertial motion.

The other modes are vorticity controlled, Rossby-like waves and are supported by two wave guides - the sloping bottom topography and the sloping isopycnals and associated shear of the mean current. The pressure (π) structure for mode 1 for wavenumber $\ell = 1.25$ is shown in Figure 5.2(a). Figures 5.2(b) and (c) show the horizontal velocities associated with this mode. In the wavenumber range $0 < \ell \leq 1.5$, this wave, consisting of a barotropic portion trapped over the shelf which co-oscillates with a baroclinic portion trapped within the frontal zone, i.e., within the region of strongly sloping isopycnals on the cyclonic side of the mean current, is a hybrid between a shelf wave and an internal Rossby-like wave. The hybrid nature of the wave decreases with increasing wavenumber, that is, the barotropic component over the shelf diminishes. For intermediate wavenumbers ($1.5 \leq \ell \leq 3.5$), this mode becomes a "frontal-trapped" wave with most of the energy trapped within the frontal zone (Figure 5.3). As the wavenumber increases still further, the hybrid structure over the shelf returns and

the frontal-trapped wave begins to die out. For wavenumber: $\ell \geq 3.75$, the frontal-trapped structure is completely gone, and this mode becomes a topographic Rossby wave (Figure 5.4).

Mode 2 for low wavenumbers is a topographic Rossby wave over the shelf that dies out in the frontal zone. The pressure and velocity structures for this mode are shown in Figure 5.5. For higher wavenumbers ($\ell \geq 3.75$) this mode begins to exhibit baroclinic structure in the frontal zone and becomes a hybrid wave (Figure 5.6). It therefore appears that modes 1 and 2 exchange characteristics around $\ell = 3.75$. This is similar to the resonance coupling found by Bane (1980) in a two-layer Gulf Stream model. Mode 3 is a hybrid wave for all wavenumbers considered (Figure 5.7), while mode 4 exhibits the frontal-trapped structure (Figure 5.8).

Aside from the single internal Kelvin wave mode, there appear to be three distinctly different wave structures. The first is a topographic Rossby wave, which is confined to the shelf region (i.e., a continental shelf wave) and dies out in the frontal zone of the mean current. The second is the frontal-trapped wave, which is essentially an internal Rossby wave supported by the vorticity gradient resulting from the sloping density surfaces and shear associated with the mean current. Over the shelf, where the stratification is level, there is very little motion associated with this wave. The third type of wave is a hybrid between the first two and has components over the shelf and in the current region that are of comparable magnitude. These three structures can be understood by considering the potential vorticity control mechanisms which support the wave motion. For barotropic motions

over a sloping bottom, conservation of potential vorticity dictates that

$$\frac{D}{Dt} \left(\frac{\xi+f}{h} \right) = 0 \quad (5.1)$$

where $\xi = v_x - u_y$ is the vertical component of the relative vorticity of the wave motion. This is the case over the shelf; therefore, the wave vorticity can be balanced only by the topographic background vorticity f/h and only topographic Rossby waves are allowed. The effect of a level stratification is to concentrate this background vorticity gradient in the lower layers, leading to bottom trapping of the wave motion, as in Figure 5.5.

The presence of a mean current with both lateral and vertical shear gives an additional vorticity constraint, the conservation of quasi-geostrophic potential vorticity (cf, Pedlosky, 1979)

$$\frac{DQ}{Dt} = \frac{D}{Dt} \left[(\omega + f\hat{k}) \cdot \frac{\nabla \rho}{\rho_0} \right] = 0 \quad (5.2)$$

where $\omega = \nabla \times (u\hat{i} + (v+\bar{v})\hat{j} + w\hat{k})$ is the total vorticity vector. The wave vorticity can now be balanced by the background quasi-geostrophic potential vorticity

$$\begin{aligned} \bar{Q} &= (\bar{f}\hat{k} - \bar{v}_z\hat{j}) \cdot \frac{\nabla \rho}{\rho_0} \\ &= \frac{M^2}{g} \bar{v}_z - \frac{N^2}{g} \bar{f} \end{aligned} \quad (5.3)$$

(where $\bar{f} = (f + \bar{v}_x)$), or from the thermal wind relation

$$\bar{Q} = \frac{1}{fg} \left(M^4 - N^2 \sigma_f^2 \right). \quad (5.4)$$

This quantity is plotted in Figure 5.9. The quasi-geostrophic potential vorticity balance is then

$$\frac{D}{Dt} (\bar{Q} + Q') = 0$$

where $Q' = \epsilon \frac{\bar{\rho}_z}{\rho_0} + (w_y - v_z) \frac{\bar{\rho}_x}{\rho_0}$ is the wave quasi-geostrophic vorticity. The current alone can support internal Rossby waves due to the gradient in \bar{Q} . This gradient is strongest near the surface in the frontal zone; hence, the wave motion may be concentrated there. The strong density stratification in the current effectively isolates these waves from the bottom topography for all but the very longest wavelengths. This can be seen by comparing Figures 5.2(a) and Figure 5.3. Mode 1 shows a strong bottom-trapped component at $\ell = 1.25$ (Figure 5.2(a)) which disappears at $\ell = 2.0$ (Figure 5.3).

For a level, two layer stratification over bottom topography, Allen (1975) has shown that the strength of the coupling between barotropic and baroclinic modes depends on a parameter $\lambda = r_i / \delta_B$,

where $r_i = \frac{NH}{f}$ is the internal Rossby radius of deformation and $\delta_B = H/H_x$ is a length scale for the bottom topography. Over the shelf in the present model, $N \sim 4 \times 10^{-3} \text{ sec}^{-1}$, $H \sim 10^2 \text{ m}$, $f \sim 10^{-4} \text{ sec}^{-1}$ and $\delta_B \sim 100 \text{ km}$, so that $r_i \sim 4 \text{ km}$ and $\lambda \sim 0.004$. In the current, however, $N \sim 5 \times 10^{-3} \text{ sec}^{-1}$, $H \sim 1000 \text{ m}$ and $r_i \sim 50 \text{ km}$, giving $\lambda \approx 0.5$. This

parameter was derived for a level stratification and is not totally applicable here. As shown above, the presence of sloping isopycnals permits the frontal-trapped wave motion that does not exist in a level stratification. Coupling between this type of motion and waves supported by the sloping topography is another matter. If the phase speeds of the frontal-trapped wave and the topographic Rossby wave are similar for a given wavelength, the two waves can co-oscillate, resulting in a hybrid wave. Otherwise, only one type of wave may exist.

The phase speeds for modes 1, 2 and 3 at low wavenumbers are very close to the first three barotropic shelf wave speeds for the same depth profile. This is to be expected, since for very long waves, $\frac{\partial}{\partial y}$, u' and w' in (2.3) through (2.7) become small. Each mode (excluding the internal Kelvin wave mode) has a high frequency cutoff, resulting in a zero group speed point for each mode. Table 5.1 gives the values of the cutoff frequency σ_c , the corresponding wavenumber, and the phase speed associated with the zero group speed of each mode for the first three Rossby-like wave modes. The higher-order wave modes are not adequately resolved by the solution method.

Table 5.1. Values for high frequency cutoff, σ_c for the first three Rossby-like wave modes.

Mode	σ_c	Dimensional Frequency	ℓ	Dimensional Wavelength	Dimensional Phase Speed
1	0.324	$2.62 \times 10^{-5} \text{sec}^{-1}$	2.25	558.5 km	200 km/day
2	0.223	$1.804 \times 10^{-5} \text{sec}^{-1}$	3.7	339.6 km	84 km/day
3	0.15	$1.21 \times 10^{-5} \text{sec}^{-1}$	4.13	304.3 km	50 km/day

6. Discussion

One usually thinks of a wave mode in terms of a specific modal structure; for instance, the number of nodes in the horizontal or vertical pressure structure. This concept of modal structure does not seem to apply to the modes found in the present model. Each mode is a composite of several different wave structures, with a particular mode exhibiting different structures in different regions of the dispersion plane. Modes 1 and 2 show a coupling resonance phenomenon, wherein the two modes exchange characteristics. The term "resonance", which was first used in this context by Eckart (1962), is somewhat misleading since there is no infinite growth in the wave amplitude (cf Allen, 1975).

Similar phenomena have been observed in other coastal-trapped wave models. Niiler and Mysak (1971) found that the dispersion curves for their shelf wave modes and shear wave modes change families where the curves appear to cross. Allen (1975), Wang (1975) and Wang and Mooers (1976) found similar coupling between topographic Rossby wave modes and internal Kelvin wave modes in models that included a level stratification over a sloping topography. Bane (1980), in a two-layer Gulf Stream model, found that the dispersion curves for a particular topography/density/current setting may be interpreted as a composite of the families of dispersion curves of the four different wave types present in the model. These four wave types are the barotropic shelf waves, the barotropic quasigeostrophic edge waves, the complementary mode edge waves and the frontal-trapped waves. In the present continuously stratified model, these four types of waves are not as easily distinguished as they are in Bane's (1980) model. This is due to the

fundamental difference between a two-layer stratification and a continuous stratification. In the two-layer case, all the density information is contained in a single discontinuity; whereas in the continuously stratified case, the density information is distributed over the entire water column, giving much greater vertical resolution. Thus, the interactions between stratification and topography are much more subtle. It is important to note that one cannot speak of the mean velocity and mean density fields independently, as they are intimately coupled through the thermal wind relation. In this particular model, the mean density field was specified and the mean velocity field was computed from it; however, one could have just as easily specified the mean velocity field and then computed the associated density field. Therefore, when we speak of the mean current or the mean stratification, we are referring to both the mean velocity and density fields.

The barotropic shelf wave dispersion curves were computed for the model bottom topography and are shown in Figure 6.1. Comparing these curves with those of Figure 5.1, it is clear that the presence of the mean current significantly alters the propagation of the shelf waves. For very long wavelengths ($\ell < 0.5$) both sets of curves are roughly coincident. This is to be expected, since for very long wavelengths $\frac{\partial}{\partial y}$, u , and w in (2.3) - (2.7) become very small in relation to the other terms. For smaller wavelengths (larger wavenumber) the dispersion curves for the stratified model are quite different from the barotropic curves. It is not clear at present how the barotropic curves make the transition to the stratified curves. This question will be addressed in future work.

The two-layer model of Bane (1980) has shown that the location of the density front in relation to the topography is very important in determining the dispersion properties of the various waves. It is expected that the same is true of the continuously stratified case; however, this has not yet been investigated.

The horizontal resolution of the numerical method employed in this model was not quite as good as desired. Much of the complex structure in Figures 5.2 through 5.7 resulted from contouring only a few mesh points, and should therefore be viewed as merely suggestive of the true wave structure. A new numerical method has been recently developed at NCAR that should improve the resolution of this model by an order of magnitude in future computations.

This study has only considered small amplitude, stable perturbations to the basic state. The problems of baroclinic instability and critical levels in the mean flow have been excluded in order to simplify the analysis. Inspection of the quasigeostrophic potential vorticity field (Figure 5.8) reveals that the potential vorticity gradient changes sign seaward of the frontal zone. This is a necessary, but not a sufficient, condition for baroclinic instability (cf Pedlosky, 1979, p. 440); therefore, unstable waves are possible, but a more detailed analysis is required to determine the exact form of the perturbations for which the flow is unstable.

Recent measurements in the Gulf Stream south of Cape Hatteras indicate that a dominant mode of oscillation of the Stream corresponds to a downstream propagating disturbance with a period of eight days (Bane and Brooks, 1979b; Brooks and Bane, 1980). The present model,

however, only considers upstream propagating disturbances, and thus avoids the possibility of critical levels in the flow. A logical extension of this model would be to consider downstream propagating waves and unstable waves by allowing the wave frequency σ_0 to assume negative and complex values.

The vertical wall imposed at the coast is not a very realistic boundary condition. The Kelvin wave mode (mode 0) is purely a consequence of this boundary condition. The vertical wall requires a node in the cross-shelf velocity at the coast. A more realistic sloping beach boundary condition would only require that the solution remain bounded at the coast; however, this would be much more difficult to treat numerically. Bane (1980) compared the sloping beach and vertical wall boundary conditions in the two-layer case and found that the vertical wall did not affect the solutions appreciably so long as the wall was of small height compared to the total depth and was far removed from the frontal zone.

7. Conclusions

It has been shown that the presence of a continuously stratified boundary current such as the Gulf Stream in a coastal-trapped wave model permits the existence of a new class of frontal-trapped waves in addition to the topographic Rossby wave (continental shelf wave) modes. The frontal-trapped wave is a Rossby-like wave in that it is supported by the ambient quasi-geostrophic potential vorticity gradient in the cyclonic side of the mean current. This potential vorticity gradient is due to both the shear of the mean current and the associated sloping density surfaces. Bane (1980) also has found frontal-trapped waves in a two-layer Gulf Stream model. In the present model, the mean current flows along the continental slope, with its inshore surface front located approximately over the shelf break. The wide continental shelf simulates the topography off Onslow Bay, North Carolina. The stratification over the shelf is level, so that only topographic Rossby waves may exist there. Frontal-trapped waves may exist in the frontal zone of the mean current. These two regions are coupled, and the resulting wave motion may be either a shelf wave, a frontal-trapped wave, or a hybrid between the two. Following a particular dispersion curve, the modal structure changes from one wave form to another, indicating a mode-coupling resonance similar to that found by Bane (1980). The coupling between the two wave guides (the topographic potential vorticity gradient and the quasi-geostrophic potential vorticity gradient) is much more subtle in the continuously stratified case than in the two layer case. It is inappropriate to speak of a particular modal structure in the continuous case, since a wave mode exhibits different structures in

different regions of the dispersion plane.

The importance of these stable Rossby-like waves to the mesoscale variability of the real Gulf Stream is not known. The free modes found in this model reveal a possible mechanism for sub-inertial frequency disturbances propagating along the inshore side of the Stream. The complexity of the solutions in this highly simplified model of the Gulf Stream indicate that the response of the real Stream depends upon a number of interacting factors.

Acknowledgments

We would like to express our deepest appreciation to Dr. Patrick J. Roache for generously providing the subroutine used in solving the governing equation. Our thanks also go to the staff of the Computing Facility at the National Center for Atmospheric Research in Boulder, Colorado, for their invaluable assistance.

This research was supported by the U. S. Navy Office of Naval Research under contract number N00014-77-C-0354, and by the National Science Foundation under grant number OCE-7923413 through the Curriculum in Marine Sciences of the University of North Carolina at Chapel Hill. Computing services were provided by the National Center for Atmospheric Research, which is sponsored by the National Science Foundation.

Appendix

A1. Separation of time dependent flow from mean flow

The full equations of motion are

$$Du - fv = -\frac{1}{\rho} p_x + \nu \nabla^2 u \quad (\text{A1.1})$$

$$Dv + fu = -\frac{1}{\rho} p_y + \nu \nabla^2 v \quad (\text{A1.2})$$

$$Dw + ew = -\frac{1}{\rho} p_z - g + \nu \nabla^2 w \quad (\text{A1.3})$$

$$\frac{1}{\rho} D\rho + \nabla \cdot \bar{q} = 0 \quad (\text{A1.4})$$

where

$$D = \frac{\partial}{\partial t} + u \frac{\partial}{\partial x} + v \frac{\partial}{\partial y} + w \frac{\partial}{\partial z}$$

$$\bar{q} = u\hat{i} + v\hat{j} + w\hat{k}$$

f is the vertical component of the earth's rotation, which will be assumed constant,

e is the horizontal component of the earth's rotation, which will be assumed negligible,

and ν is the molecular viscosity. Henceforth, the fluid will be assumed inviscid, i.e. $\nu = 0$. Equation (A1.4) can be separated into two equivalent equations because the fluid is incompressible:

$$D\rho = 0 \quad (\text{A1.5})$$

$$u_x + v_y + w_z = 0 \quad (\text{A1.6})$$

The dependent variables consist of a mean or time-independent component and a fluctuating or time-dependent part. The mean velocity is in the y-direction only, so that the mean velocity components in the x and z directions are zero:

$$u = u', \quad v = \bar{v} + v', \quad w = w'$$

$$p = p_0 + \bar{p} + p', \quad \rho = \rho_0 + \bar{\rho} + \rho'$$

where $p_0 = \rho_0 g z$ is the hydrostatic pressure.

The equations of motion are averaged over a period of time much greater than a typical time scale for the time-dependent motions, i.e.

$$\bar{r} = \frac{1}{T} \int_{\tau - \frac{T}{2}}^{\tau + \frac{T}{2}} r \, dt, \quad r \text{ any dependent variable.}$$

A Boussinesq approximation is adopted, that is, $(\bar{\rho}, \rho') \ll \rho_0$ so that ρ is replaced by ρ_0 everywhere except in the buoyancy equation (A1.5).

The mean flow equations are then

$$f\bar{v} = \frac{1}{\rho_0} \bar{p}_x + \left[\overline{u'u'}_x + \overline{v'u'}_y + \overline{w'u'}_z \right] \quad (\text{A1.7})$$

$$0 = \frac{1}{\rho_0} \bar{p}_y + \left[\overline{u'v'}_x + \overline{v'v'}_y + \overline{w'v'}_z \right] \quad (\text{A1.8})$$

$$0 = \frac{1}{\rho_0} \bar{p}_z + g + \left[\overline{u'w'}_x + \overline{v'w'}_y + \overline{w'w'}_z \right] \quad (\text{A1.9})$$

The terms in brackets are the x, y and z components of the Reynolds stress and will be denoted as $R^{(x)}$, $R^{(y)}$ and $R^{(z)}$, respectively. The

buoyancy is defined as

$$b = -\frac{g\rho}{\rho_0} = b_0 + \bar{b} + b'$$

and the non-hydrostatic pressure per unit density as

$$\pi = \frac{p-p_0}{\rho_0} = \bar{\pi} + \pi'$$

Equations (A1.7) through (A1.9) now become

$$f\bar{v} = \bar{\pi}_x + R^{(x)} \quad (\text{A1.10})$$

$$0 = \bar{\pi}_y + R^{(y)} \quad (\text{A1.11})$$

$$0 = \bar{\pi}_z - b + R^{(z)} \quad (\text{A1.12})$$

Equations (A1.10) through (A1.12) are added to (A1.1) through (A1.3) to give the equations of motion for the time dependent flow:

$$u'_t + \bar{v}u'_y + u'u'_x + v'u'_y + w'u'_z - fv' = -\pi'_x + R^{(x)} \quad (\text{A1.13})$$

$$\begin{aligned} v'_t + \bar{v}v'_y + u'v'_x + v'v'_y + w'v'_z + fu' + \bar{v}_x u' + \bar{v}_z w' \\ = -\pi'_y + R^{(y)} \end{aligned} \quad (\text{A1.14})$$

$$w'_t + \bar{v}w'_y + u'w'_x + v'w'_y + w'w'_z = -\pi'_z + b' + R^{(z)} \quad (\text{A1.15})$$

$$u'_x + v'_y + w'_z = 0 \quad (\text{A1.16})$$

$$b'_t + \bar{v}b'_y + M^2 u' + N^2 w' + u'b'_x + v'b'_y + w'b'_z = 0 \quad (\text{A1.17})$$

Equations (A1.13) through (A1.17) are the full non-linear equations for the wave motion. In this analysis, the non-linear terms and the Reynolds stresses are assumed to be small compared to the other terms in the equations. This can be verified through a simple scale analysis (cf, Brooks, 1975, pp. 212-218). A hydrostatic approximation is adopted, since the vertical velocity w is small, and its derivatives for long waves are smaller still when compared to the pressure and buoyancy terms. The linearized, hydrostatic equations for the wave motion, with the primes dropped, are

$$u_t + \bar{v}u_y - fv = -\pi_x \quad (\text{A1.18})$$

$$v_t + \bar{v}v_y + (f + \bar{v}_x)u + \bar{v}_z w = -\pi_y \quad (\text{A1.19})$$

$$0 = -\pi_z + b \quad (\text{A1.20})$$

$$u_x + v_y + w_z = 0 \quad (\text{A1.21})$$

$$b_t + \bar{v}b_y + M^2 u_x + N^2 w = 0 \quad (\text{A1.22})$$

A2. Formulation of the governing equation.

The equations of motion for the mean flow can be combined by differentiating (A1.10) with respect to z and (A1.12) with respect to x , and subtracting to give the thermal wind relation

$$f\bar{v}_z = M^2, \quad (\text{A2.1})$$

which will be applied numerous times in this section.

Alongshore propagating disturbances are sought; therefore the perturbation variables are taken to have the form $e^{i(\sigma_0 t + \ell y)}$ as their (y, t) dependence. The equations of motion (A1.18) through (A1.22) now become

$$i\sigma u - f v = -\pi_x \quad (\text{A2.2})$$

$$i\sigma v + (f + \bar{v}_x)u + \bar{v}_z w = -i\ell\pi \quad (\text{A2.3})$$

$$0 = -\pi_z + b \quad (\text{A2.4})$$

$$u_x + i\ell v + w_z = 0 \quad (\text{A2.5})$$

$$i\sigma b + M^2 u + N^2 w = 0 \quad (\text{A2.6})$$

where $\sigma = \sigma_0 + \bar{v}\ell$ is the intrinsic frequency.

Eliminating the buoyancy b between (A2.4) and (A2.6) gives

$$M^2 u + N^2 w = -i\sigma\pi_z \quad (\text{A2.7})$$

Using this result to eliminate w from (A2.3) gives

$$\sigma N^2 v - i [N^2 (f + \bar{v}_x) - M^2 \bar{v}_z] u = -\ell N^2 \pi + \sigma \bar{v}_z \pi_z \quad (\text{A2.8})$$

Using (A2.2) to eliminate v in (A2.8) and applying the thermal wind relation (A2.1) gives

$$u = \frac{\sigma N^2}{i \Delta} \left(\pi_x - \frac{M^2}{N^2} \pi_z + \frac{\ell f}{\sigma} \pi \right) \quad (\text{A2.9})$$

where $\Delta = N^2 (\sigma_f^2 - \sigma^2) - M^4$ and $\sigma_f^2 = f(f + \bar{v}_x)$. Solving for v by eliminating u between (A2.2) and (A2.8) gives

$$v = \frac{1}{f \Delta} \left[(N^2 \sigma_f^2 - M^4) \pi_x - \sigma^2 M^2 \pi_z + \sigma f \ell N^2 \pi \right] \quad (\text{A2.10})$$

The vertical velocity w is found by using equation (A2.7) and (A2.9):

$$w = \frac{i \sigma}{\Delta} \left[M^2 \pi_x - (\sigma_f^2 - \sigma^2) \pi_z + \frac{M^2 \ell f}{\sigma} \pi \right] \quad (\text{A2.11})$$

Substituting (A2.9), (A2.10) and (A2.11) into the continuity equation (A2.5) gives the governing equation

$$\begin{aligned} & \left[\frac{-\sigma N^2}{\Delta} \left(\pi_x - \frac{M^2}{N^2} \pi_z + \frac{\ell f}{\sigma} \pi \right) \right]_x \\ & + \frac{\ell}{f \Delta} \left[(N^2 \sigma_f^2 - M^4) \pi_x - \sigma^2 M^2 \pi_z + \sigma f \ell N^2 \pi \right] \\ & + \left[\frac{\sigma}{\Delta} \left\{ M^2 \pi_x - (\sigma_f^2 - \sigma^2) \pi_z + \frac{M^2 \ell f}{\sigma} \pi \right\} \right]_z = 0 \end{aligned} \quad (\text{A2.12})$$

After carrying through the differentiations, rearranging, and using the identities

$$N_x^2 = M_x^2 \cdot (\sigma_f^2)_z = M_x^2$$

$$\sigma_z = \frac{\ell}{f} M^2, \quad \sigma_z^2 = \frac{2\sigma\ell M^2}{f}$$

$$\sigma_x = \frac{\ell}{f} (\sigma_f^2 - f^2) = \bar{v}_x \ell$$

all of which follow from the thermal wind relation (A2.1), the governing equation becomes

$$\begin{aligned} \pi_{xx} - \frac{2M^2}{N^2} \pi_{xz} + \frac{(\sigma_f^2 - \sigma^2)}{N^2} \pi_{zz} + \frac{1}{\Delta} \left(\frac{M^2}{N^2} \frac{\partial \Delta}{\partial z} - \frac{\partial \Delta}{\partial x} \right) \pi_x \\ + \left[\frac{1}{\Delta} \left\{ \frac{M^2}{N^2} \frac{\partial \Delta}{\partial x} - \frac{(\sigma_f^2 - \sigma^2)}{N^2} \frac{\partial \Delta}{\partial z} \right\} - \frac{2\sigma\ell}{f} \frac{M^2}{N^2} \right] \pi_z \\ + \left[\frac{\ell f}{\sigma} \left(\frac{M^2}{N^2} \frac{\partial \Delta}{\partial z} - \frac{\partial \Delta}{\partial x} \right) - \ell^2 \right] = 0 \end{aligned} \quad (\text{A2.13})$$

The discriminant of (A2.13) is

$$\Gamma = 4 \frac{M^4}{N^4} - \frac{(\sigma_f^2 - \sigma^2)}{N^2} \quad (\text{A2.14})$$

which is negative for the density profile considered in this study as long as $\sigma_0 < f$; therefore the governing equation is elliptic.

A3. Finite difference form of the forced equation

The governing equation (2.25) has the general form

$$A\Pi_{xx} + B\Pi_{x\zeta} + C\Pi_{\zeta\zeta} + D\Pi_x + E\Pi_\zeta + F\Pi = 0 \quad (\text{A3.1})$$

where A, B, C, D, E, and F are functions of $(x, \zeta; \sigma_0, \ell)$. If we consider Π to consist of a perturbation pressure π , plus a constant forcing term τ , then the forced equation is

$$A\pi_{xx} + B\pi_{x\zeta} + C\pi_{\zeta\zeta} + D\pi_x + E\pi_\zeta + F\pi = -F\tau \quad (\text{A3.2})$$

This forcing term is equivalent to forcing the system by

$$\tau e^{i(\sigma_0 t + \ell y)}$$

and is used only to search for the resonance response of the system.

The usual second-order accurate, centered difference analogues of the derivative terms are used for the finite difference form of (A3.2):

$$\begin{aligned} & \frac{A_{ij}}{\Delta x^2} (\pi_{i+1,j} - 2\pi_{i,j} + \pi_{i-1,j}) \\ & + \frac{B_{ij}}{4\Delta x \Delta \zeta} (\pi_{i+1,j+1} - \pi_{i-1,j+1} - \pi_{i+1,j-1} + \pi_{i-1,j-1}) \\ & + \frac{C_{ij}}{\Delta^2 \zeta} (\pi_{i,j+1} - 2\pi_{i,j} + \pi_{i,j-1}) \\ & + \frac{D_{ij}}{2\Delta x} (\pi_{i+1,j} - \pi_{i-1,j}) + \frac{E_{ij}}{2\Delta \zeta} (\pi_{i,j+1} - \pi_{i,j-1}) \\ & + F_{ij} \pi_{ij} = G_{ij} \end{aligned} \quad (\text{A3.3})$$

where $A_{ij} = A(x_i, \zeta_j; \sigma_0, \ell)$ etc.; $G_{ij} = -F_{ij}\tau$;

$$\Delta x = \frac{x_{\max}}{I-1}, \quad \Delta \zeta = \frac{\zeta_{\max}}{J-1}, \quad \text{and } I \text{ and } J \text{ are the number of}$$

grid points in the x and ζ directions, respectively.

Some rearrangement leads to

$$\begin{aligned} & \frac{-B_{ij}}{4\Delta x \Delta \zeta} \pi_{i-1, j+1} + \left(\frac{C_{ij}}{\Delta \zeta^2} + \frac{E_{ij}}{2\Delta \zeta} \right) \pi_{i, j+1} + \frac{B_{ij}}{4\Delta x \Delta \zeta} \pi_{i+1, j+1} \\ & + \left(\frac{A_{ij}}{\Delta x^2} - \frac{D_{ij}}{2\Delta x} \right) \pi_{i-1, j} + \left[F_{ij} - 2 \left(\frac{A_{ij}}{\Delta x^2} + \frac{C_{ij}}{\Delta \zeta^2} \right) \right] \pi_{ij} \\ & \quad + \left(\frac{A_{ij}}{\Delta x^2} + \frac{D_{ij}}{2\Delta x} \right) \pi_{i+1, j} \\ & + \frac{B_{ij}}{4\Delta x \Delta \zeta} \pi_{i-1, j-1} + \left(\frac{C_{ij}}{\Delta \zeta^2} - \frac{E_{ij}}{2\Delta \zeta} \right) \pi_{i, j-1} + \left(\frac{-B_{ij}}{4\Delta x \Delta \zeta} \right) \pi_{i+1, j-1} = G_{ij} \end{aligned} \tag{A3.4}$$

This is a nine-point stencil over the interior grid points, that is, for $i = 2$ to $I-1$ and $j = 2$ to $J-1$ (See Figure A3.1).

This equation is solved using the FORTRAN subroutine EVP9G, generously provided by Pat Roache. The subroutine utilizes the Error Vector Propagation (EVP) algorithm described in Roache (1978). Given the coefficients for the finite difference equation (A3.4) and the coefficients for the boundary conditions, EVP9G returns the solution for π .

The boundary conditions (2.26) through (2.28) are of the form

$$A_{nb} \pi_x + B_{nb} \pi_\zeta + C_{nb} \pi = 0 . \quad (\text{A3.5})$$

For the bottom and top boundary conditions (subscript $nb = 1, 2$ respectively), EVP9G uses the second-order accurate finite difference approximation for the x derivative but allows only a first-order approximation to the normal gradient. A second-order form is possible but would require a bi-tridiagonal matrix solution to start the march.

At the inshore boundary ($nb = 3$) both the depth and the stratification are very small; therefore, to greatly simplify the computations, π_ζ is taken to be zero. The boundary condition then becomes

$$\frac{\pi_x}{\pi} = \frac{-C_3}{A_3}$$

Again, the finite difference approximation to the normal gradient is only accurate to first order.

The offshore boundary condition ($nb = 4$) is a simple Dirichlet condition and its values are stored in $\pi_{I,j}$ when EVP9G is called.

A4. Subroutine EVP9G (INIT, F, C1, C2, C3, C4, C5, C6, C7, C8, C9, C10,
IL, JL, ILD, NCRS, NBJ1, NBJL, CTA, CTB, CTC, CBA,
CBB, CBC, NB11, CLEF)

This subroutine solves the equation

$$\begin{aligned} &C1(I,J)*F(I-1,J+1)+C2(I,J)*F(I,J+1)+C3(I,J)*F(I+1,J+1) \\ &+C4(I,J)*F(I-1,J)+C5(I,J)*F(I,J)+C6(I,J)*F(I+1,J) \\ &+C7(I,J)*F(I-1,J-1)+C8(I,J)*F(I,J-1) + C9(I,J)*F(I+1,J-1) = C10(I,J) \end{aligned}$$

by marching, using the EVP algorithm (see Roache, 1978)

Calling sequence:

```
CALL EVP9G(INIT, F, C1, C2, C3, C4, C5, C6, C7, C8, C9, C10, IL, JL  
ILD, NCRS, NBJ1, NBJL, CTA, CTB, CTC, CBA, CBB, CBC,  
NB11, CLEF)
```

Parameters:

INIT: Flag to determine whether the call is a repeat solution (INIT=0)
or an initialization call (INIT=1).

F: Matrix of dimension (ILD, JL). On output, F contains the solution
to the finite difference equation. If Dirichlet conditions are
used at any boundary, the boundary values are set by whatever values
are stored in the appropriate position in F when the subroutine is
called, e.g. for the offshore boundary, the values stored in
 $F(1L, J)$, $J = 1, JL$ are used as the boundary values.

C1, C2, . . . C10: Matrices of dimension (ILD, JL). On input they
contain the coefficients of the finite difference equation as
given above. The values are not changed.

- IL: Number of grid points in the x-direction. Must be less than or equal to ILD.
- JL: Number of grid points in the y-direction. Must be less than or equal to ILD.
- ILD: First dimension of F in calling program. In this version of EVP9G, ILD must be less than or equal to 31, but this can be changed by changing the appropriate dimension statements.
- NCRS: Number of cross derivatives. If $C1 = C3 = C7 = C9 = 0$, setting $NCRS = 0$ saves time in the computation. Otherwise, $NCRS = 1$, and the subroutine GTRI, a tridiagonal solver, must be made available to EVP9G. GTRI solves for the (J+1)th row in the march.
- NBJ1: Flag to determine the form of the boundary condition at the bottom ($J = 1$) boundary. $NBJ1 = 1$ gives the general oblique derivative form of the boundary condition $CBA(I)*(F(I+1,1)-F(I-1,1))+CBB(I)*(F(I,2)-F(I,1)) + CBC(I)*F(I,1) = 0$.
- $NBJ1=2$ gives simple Dirichlet conditions. In this case, the boundary values are stored in $F(I,1)$, $I = 1, IL$ on input and CBA, CBB and CBC are ignored.
- NBJL: Flag to determine the form of the boundary condition at the top ($J=JL$). Analogous to NBJ1.
- CIA, CTB, CTC: If $NBJL = 1$, arrays of length ILD containing the coefficients for the oblique derivative boundary condition at the top ($J=JL$):
- $$CIA(I)*(F(I+1,JL)-F(I-1,JL))+CTB(I)*(F(I,JL)-F(I,JL-1))$$
- $$+CTC(I)*F(I,JL) = 0$$

CBA,CBB,CBC: If NBJ1=1, arrays of length ILD containing the coefficients for the oblique derivative boundary condition at the bottom (J=1). See NBJ1 above.

NB11: Flag to determine form of boundary condition at the left boundary (I=1). For a Dirichlet condition, NB11=1, and the boundary values are stored in F(1,J), J=1, JL. For a mixed condition (sometimes called a Robin's condition), i.e.

$$F_x/F=C$$

NB11=3. This version of EVP9G does not allow oblique derivative conditions at the left boundary.

CLEF: If NB11=3, it is the constant in the finite difference form of the mixed boundary condition at the left boundary:

$$(F(2,J)-F(1,J))/F(1,J)=CLEF. \text{ Otherwise it is ignored.}$$

Precision: All arrays in the calling sequence are double precision.

Required supporting subroutines: EVP9G requires the double precision version of LINPACK matrix algebra program along with the BLAS (basic linear algebra system) which LINPACK uses. If NCRS=1, the tridiagonal solver GTRI is also required. GTRI is provided with this version of EVP9G.

Output: The solution matrix is returned in F. If the system is unstable, an error message is printed. On repeat calls (INIT=0) the maximum error and the final errors are printed.

Programming notes:

1) If the oblique derivative form of the boundary condition is used and either CTB or CBB are zero, that is, the normal gradient is not involved, a zero-divide results.

- 2) If CLEF=1.0, a zero divide will result.
- 3) The only boundary condition allowed at the right boundary is a simple Dirichlet condition.
- 4) When there is no cross-derivative term, it is not necessary to set NCRS=0, but it saves some time.

References

- Adams, J. K. and V. T. Buchwald, 1969: The generation of continental waves. J. Fluid Mech., 35, 815-826.
- Allen, J. S., 1975: Coastal trapped waves in a stratified ocean. J. Phys. Oceanogr., 5, 300-325.
- Bane, J. M., 1980: Coastal-trapped and frontal-trapped waves in a baroclinic western boundary current. J. Phys. Oceanogr., (To Appear, October).
- _____, and D. A. Brooks, 1979a: Gulf Stream meanders along the continental margin from the Florida Straits to Cape Hatteras. Geophys. Res. Letters, 6, 280-282.
- _____, and D. A. Brooks, 1979b: Three dimensional, mesoscale characteristics of the temperature field in the Gulf Stream frontal zone south of Cape Hatteras. Trans. Amer. Geophys. Union, 60, 859.
- _____, and Y. Hsueh, 1980: On the theory of coastal-trapped waves in an upwelling frontal zone. J. Phys. Oceanogr., 10, 270-285.
- Brooks, D. A., 1975: Wind-forced continental shelf waves in the Florida Current. Tech. Rept., University of Miami, Florida, 268 pp.
- _____, 1978: Subtidal sea level fluctuations and their relation to atmospheric forcing along the Carolina Coast. J. Phys. Oceanogr., 8, 481-493.
- _____, and C.N.K. Mooers, 1977a: Wind Forced Continental Shelf Waves in the Florida Current. J. Geophys. Res., 82 (18), 2569-2576.
- _____, and C.N.K. Mooers, 1977b: Free, Stable Continental Shelf Waves in a Sheared, Barotropic Boundary Current. J. Phys. Oceanogr., 7, 380-388.
- _____, and J. M. Bane, 1978: Gulf Stream deflection by a bottom feature off Charleston, South Carolina. Science, 201, 1225-1226.
- _____, and J. M. Bane, 1980: Gulf Stream meanders: Observations of their formation, structure, propagation, and energetics from Charleston to Cape Hatteras. J. Phys. Oceanogr., (Submitted).
- Buchwald, V.T., and J. K. Adams, 1968: The propagation of continental shelf waves. Proc. Roy. Soc. London, A305, 235-250.

- Cartwright, D.E., 1969: Extraordinary tidal currents near St. Kilde. Nature, 223, 928-932.
- Clarke, A. J., 1977: Observational and numerical evidence for wind-forced coastal trapped long waves. J. Phys. Oceanogr., 7, 231-247.
- Cutchin, D. L., and R. L. Smith, 1973: Continental shelf waves: low frequency variations in sea level and currents over the Oregon continental shelf. J. Phys. Oceanogr., 3, 73-82.
- Eckart, C. H., 1962: Internal waves in the ocean. Phys. Fluids, 4, 791-799.
- Gill, A. E., and A. J. Clarke, 1974: Wind-induced upwelling, coastal currents and sea level changes. Deep-Sea Res., 21, 325-345.
- _____, and E. H. Schumann, 1974: The generation of long shelf waves by the wind. J. Phys. Oceanogr., 4, 83-90.
- Grimshaw, R., 1976: The stability of continental shelf waves in the presence of a boundary current shear, Res. Rept. No. 43, School of Mathematical Sciences, Univ. Melbourne, 19 pp.
- Hamon, B. V., 1962: The spectrums of mean sea level at Sydney, Coff's Harbor and Lord Howe Island. J. Geophys. Res., 67, 5147-5155. (Correction, 1963: J. Geophys. Res., 68, 4635).
- _____, 1966: Continental shelf waves and the effects of atmospheric pressure and wind stress on sea level. J. Geophys. Res., 71, 2883-2893.
- Huthnance, J. M., 1978: On coastal trapped waves: Analysis and numerical calculation by inverse iteration. J. Phys. Oceanogr., 8, 74-92.
- Legeckis, R.V., 1979: Satellite observations of the influence of bottom topography on the seaward deflection of the Gulf Stream off Charleston, South Carolina, J. Phys. Oceanogr., 9, 483-497,
- McKee, W.D., 1977: Continental shelf waves in the presence of a sheared geostrophic current, in Lecture Notes in Physics, vol. 64, edited by D. G. Provis and R. Radok, pp. 212-219, Australian Academy of Sciences, Canberra, and Springer-Verlag, Berlin.
- Mooers, C. N. K., 1975a: Several effects of a baroclinic current on the cross-stream propagation of inertial-internal waves. Geophysical Fluid Dynamics, 6, 245-275.
- _____, 1975b: Several effects of baroclinic currents on the three-dimensional propagation of inertial-internal waves. Geophys. Fluid Dyn., 6, 277-284.

- _____, and R. L. Smith, 1968: Continental shelf waves off Oregon. J. Geophys. Res., 73, 549-557.
- Mysak, L. A., 1967: On the theory of continental shelf waves. J. Mar. Res., 25 (3), 205-227.
- _____, 1968: Edgewaves on a gently sloping continental shelf of finite width. J. Mar. Res., 26, 24-33.
- _____, 1980: Recent advances in shelf wave dynamics. Rev. Geophys. and Space Phys., 18 (in press).
- _____, and B. V. Hamon, 1969: Low-frequency sea level behavior and continental shelf waves off North Carolina. J. Geophys. Res., 74 (6), 1397-1405.
- Niiler, P. P. and L. A. Mysak, 1971: Barotropic waves along an eastern continental shelf. Geophys. Fluid Dyn., 2, 273-288.
- Orlanski, I., 1969: The influence of bottom topography on the stability of jets in a baroclinic fluid. J. Atmos. Sci., 26, 1216-1232.
- _____, and M. D. Cox, 1973: Baroclinic instability in ocean currents. Geophys. Fluid Dyn., 4, 297-332.
- Pedlosky, J., 1979: Geophysical Fluid Dynamics, New York, Springer-Verlag, 675 pp.
- Reid, R. O., 1957: Effect of Coriolis force on edge waves. J. Mar. Res., 16, 109-141.
- Rhines, P. B., 1970: Edge-, bottom-, and Rossby waves in a rotating stratified fluid, Geophys. Fluid Dyn., 1, 273-302.
- Richardson, W. S., W. J. Schmitz, Jr., and P. P. Niiler, 1969: The velocity structure of the Florida Current from the Straits of Florida to Cape Fear. Deep-Sea Res., 16 (Suppl.), 225-231.
- Roache, P. J., 1978: Marching Methods for Elliptic Problems: Part I. Numerical Heat Transfer, 1, 1 - 25.
- Robinson, A. R., 1964: Continental shelf waves and the response of sea level to weather systems. J. Geophys. Res., 69, 367-368.
- Wang, D. P., 1975: Coastal trapped waves in a baroclinic ocean. J. Phys. Oceanogr., 5, 326-333.
- _____, and C.N.K. Mooers, 1976: Coastal-trapped waves in a continuously stratified ocean. J. Phys. Oceanogr., 6, 853-863.

Legend of Figures

- Fig. 2.1: Schematic of idealized model geometry.
- Fig. 3.1: Map of the southeastern United States coast, showing depth contours and average position of the Gulf Stream.
- Fig. 3.2: Average Gulf Stream velocity section taken off Cape Fear in summer, 1968. Contours are isotachs of downstream velocity in cm/sec. Taken from Richardson, Scmitz and Niiler (1969).
- Fig. 3.3: Model mean velocity field and bottom topography. Contours are isotachs of downstream velocity in cm/sec. Vertical and offshore coordinates are dimensionless.
- Fig. 3.4: Model mean temperature field. Contours are in degrees Celsius.
- Fig. 4.1: Solution grid. Crosses mark the grid points used in the finite difference approximation.
- Fig. 4.2: Integrated kinetic energy versus dimensionless frequency for $\ell = 2.0$. The eigenvalues of σ_0 are found by locating the local maxima of the kinetic energy.
- Fig. 4.3: Eigenvalue curves for the test case. The curves labeled I and II correspond quite well with the Mode I and Mode II topographic Rossby wave dispersion curves of Wang and Mooers (1976), which are shown in the inset as solid lines. The present model was able to resolve several other modes, in addition to those identified by Wang and Mooers (1976).

Fig. 5.1: Dispersion curves obtained from the model geometry shown in Fig. 3.3 and 3.4.

Fig. 5.2: Structure of the mode 1 wave for small wavenumber ($\ell = 1.25$). (a) Perturbation pressure π . Note the barotropic portion over the shelf transitioning to a strongly baroclinic structure in the inshore side of the mean current. Contours are in dimensionless units. (b) Alongshore velocity v , and (c) cross-shelf velocity u . Note again the strong baroclinicity in the cyclonic side of the current transitioning to a barotropic structure over the shelf. The velocity contours roughly follow constant temperature (density) surfaces (see Fig. 3.4).

Fig. 5.3: Structure of the mode 1 wave for intermediate wavenumber ($\ell = 2.0$). Shown here is the perturbation pressure π in dimensionless units. The barotropic component over the shelf is absent at this wavenumber. The mode 1 wave is a pure frontal-trapped wave at this wavenumber, with its structure confined to the surface layers on the cyclonic side of the mean current.

Fig. 5.4: Perturbation pressure π structure for the mode 1 wave for large wavenumber ($\ell = 4.0$). The frontal-trapped structure has disappeared, and this mode has become a barotropic continental shelf wave, or topographic Rossby wave.

Fig. 5.5: Structure of the mode 2 wave for intermediate wavenumber ($\ell = 2.0$). (a) Perturbation pressure π . Note the slight bottom trapping due to the density stratification. (b) Alongshore velocity v . (c) Cross-shelf velocity u .

- Fig. 5.6: Perturbation pressure π for the mode 2 wave at high wavenumber ($l = 4.0$).
- Fig. 5.7: Perturbation pressure π structure for the mode 3 wave.
- Fig. 5.8: Perturbation pressure π structure for the mode 4 wave.
- Fig. 5.9: Quasigeostrophic potential vorticity for the undisturbed mean current.
- Fig. 6.1: Barotropic shelf wave dispersion curves for the model bottom topography with no mean current or stratification.
- Fig. A3.1: (a) Nine point finite difference stencil used in solving the governing equation. (b) Schematic of solution mesh.

MODEL GEOMETRY

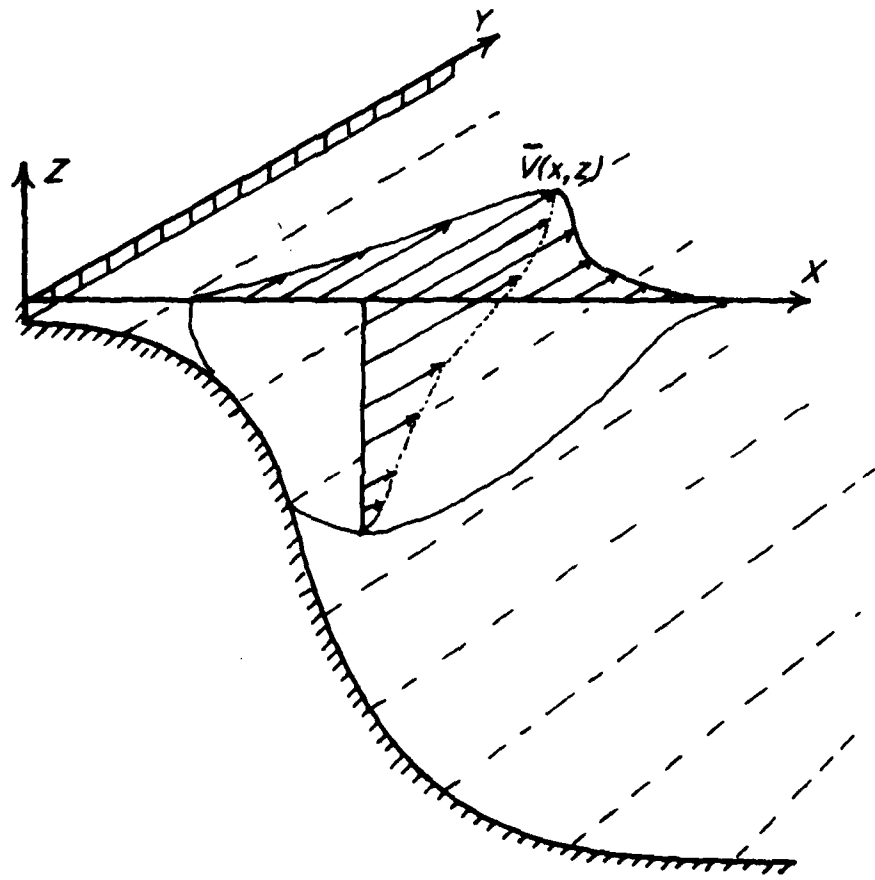


Fig. 2.1

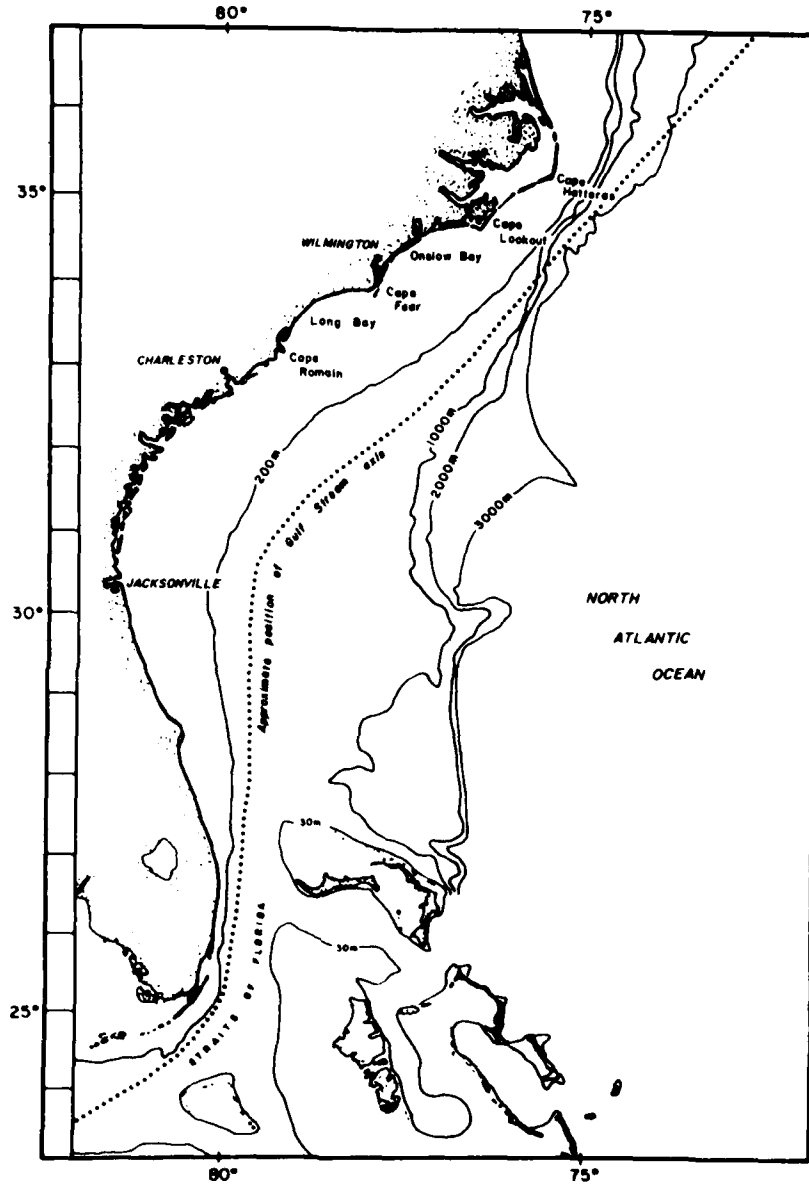


Fig. 3.1

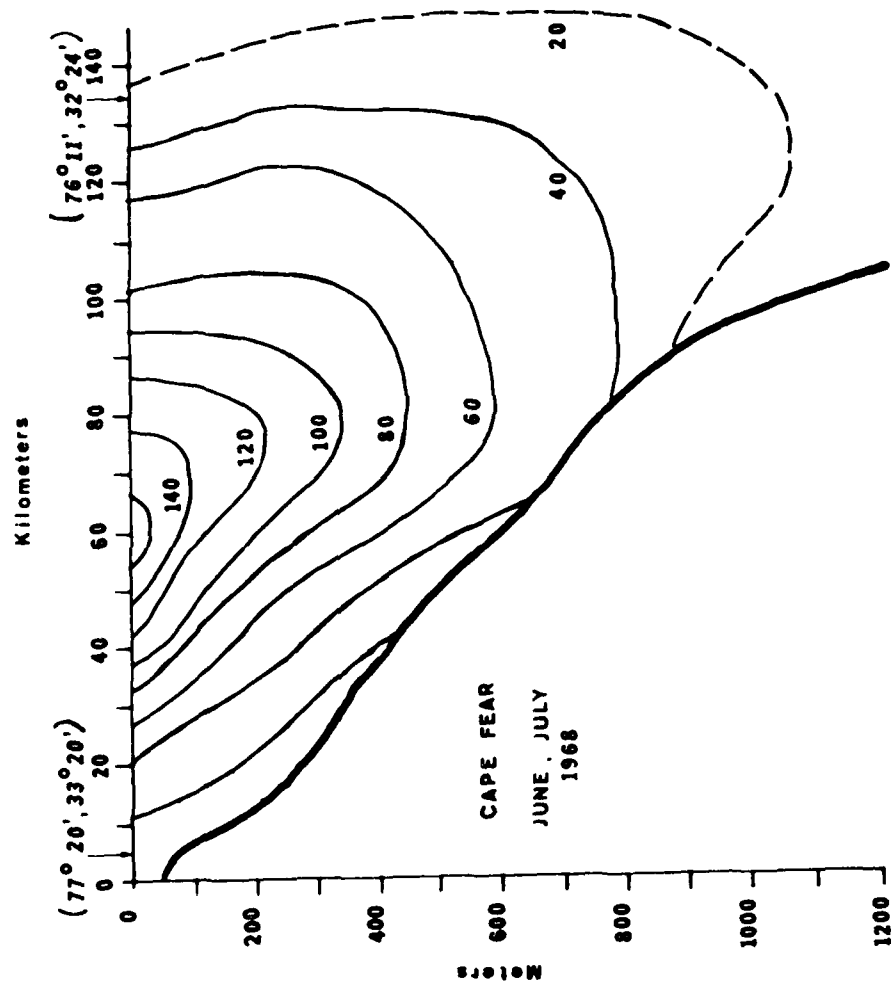


Fig. 3.2

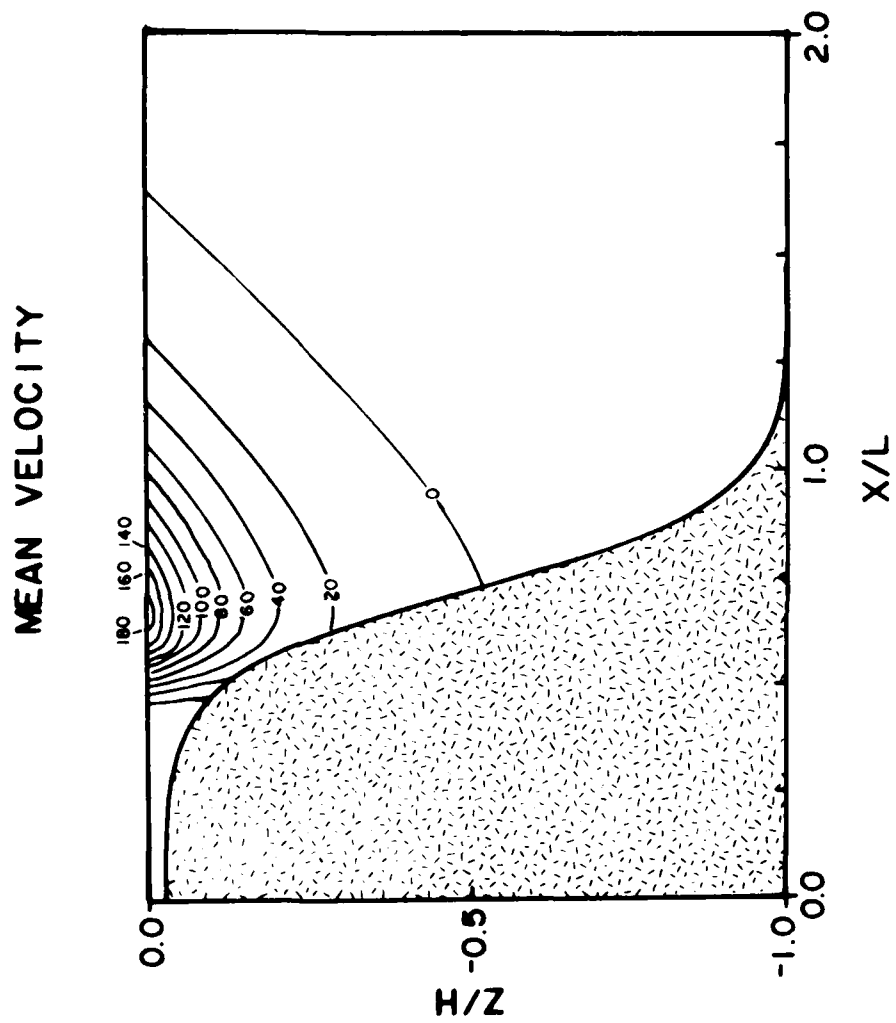


Fig. 3.3

MEAN TEMPERATURE

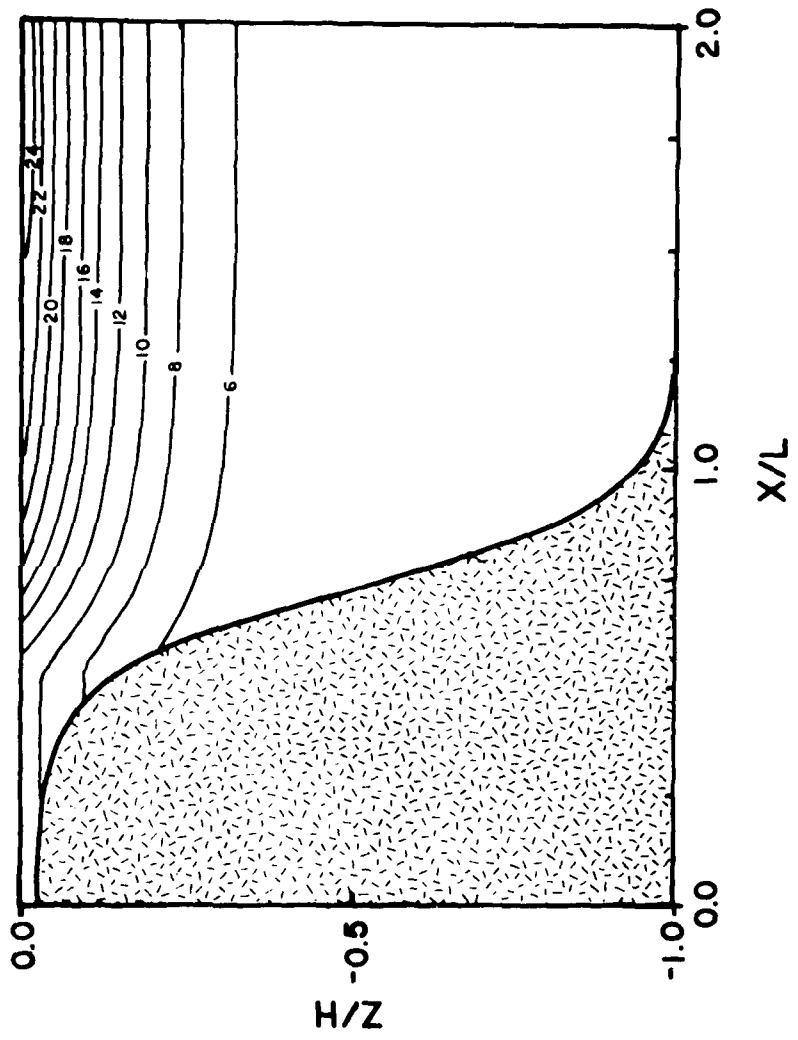


Fig. 3.4

SOLUTION MESH

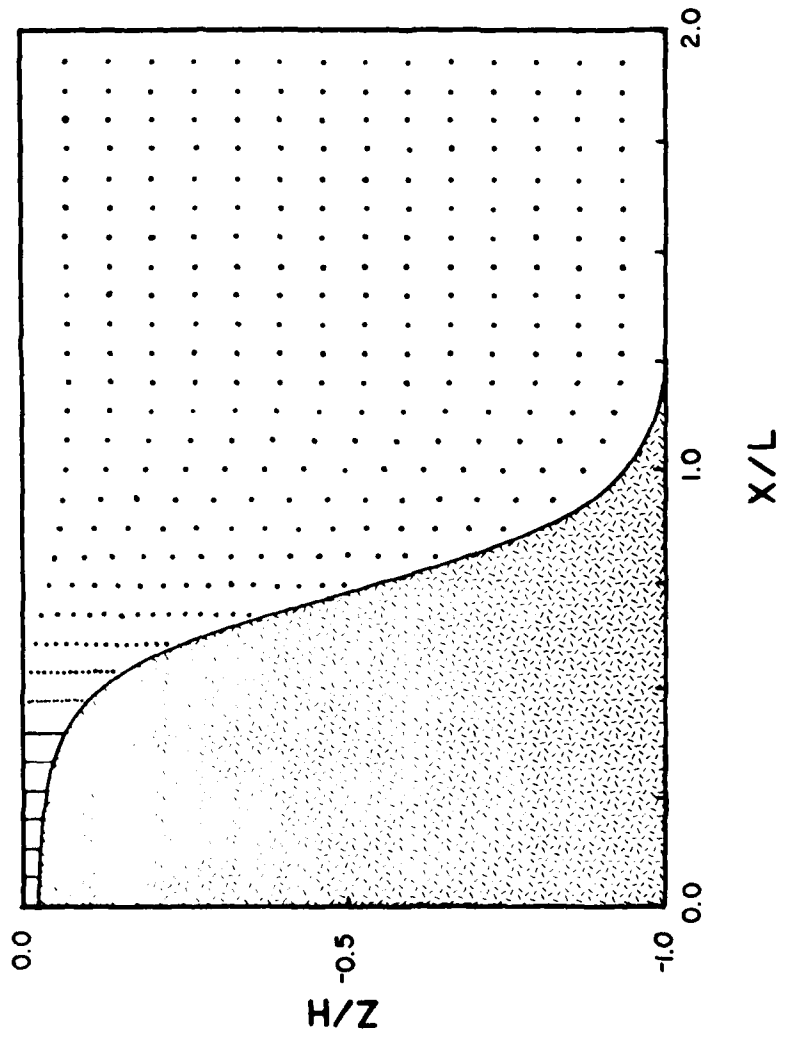


Fig. 4.1

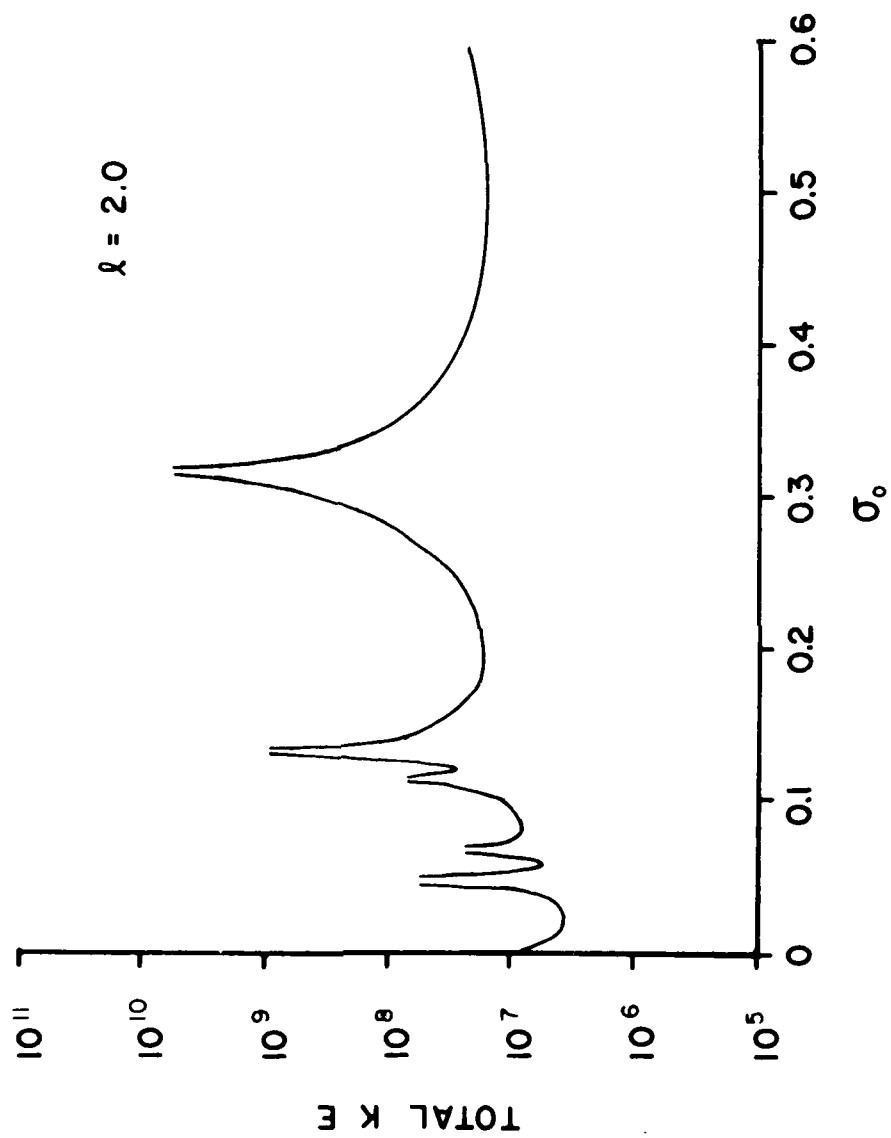


Fig. 4.2

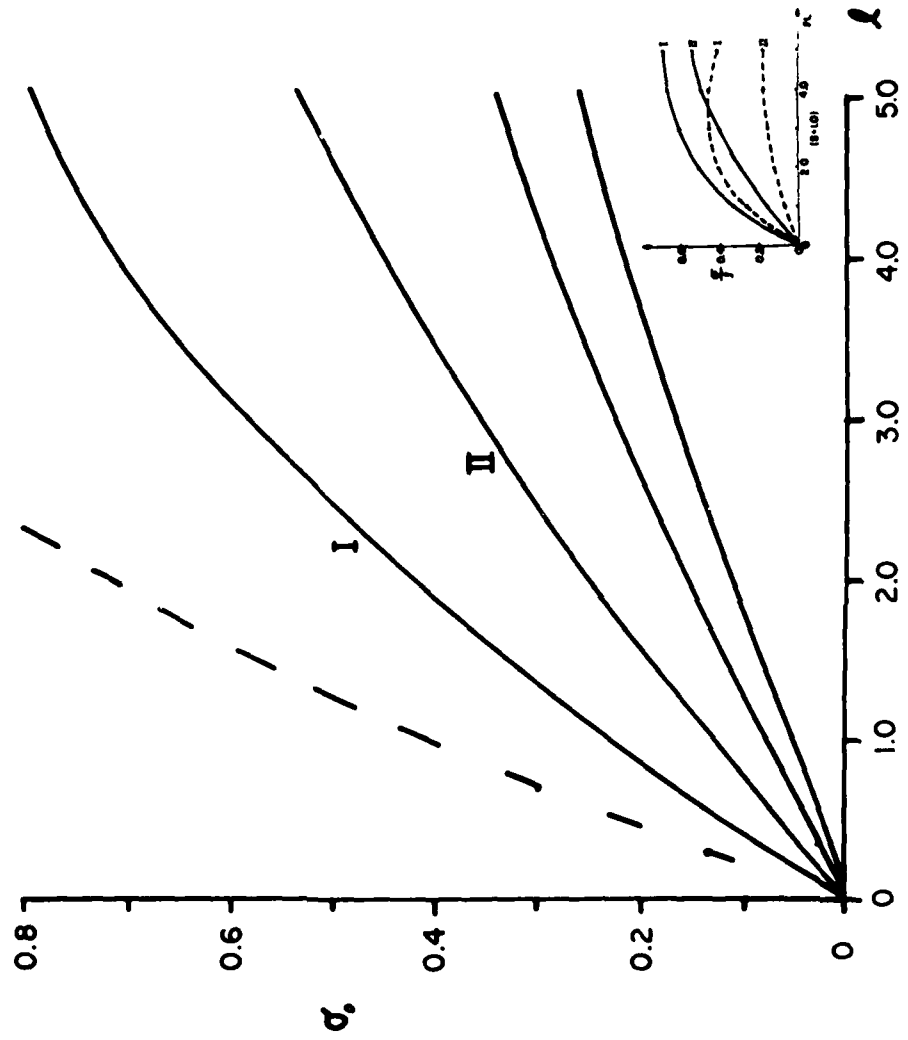


Fig. 4.3

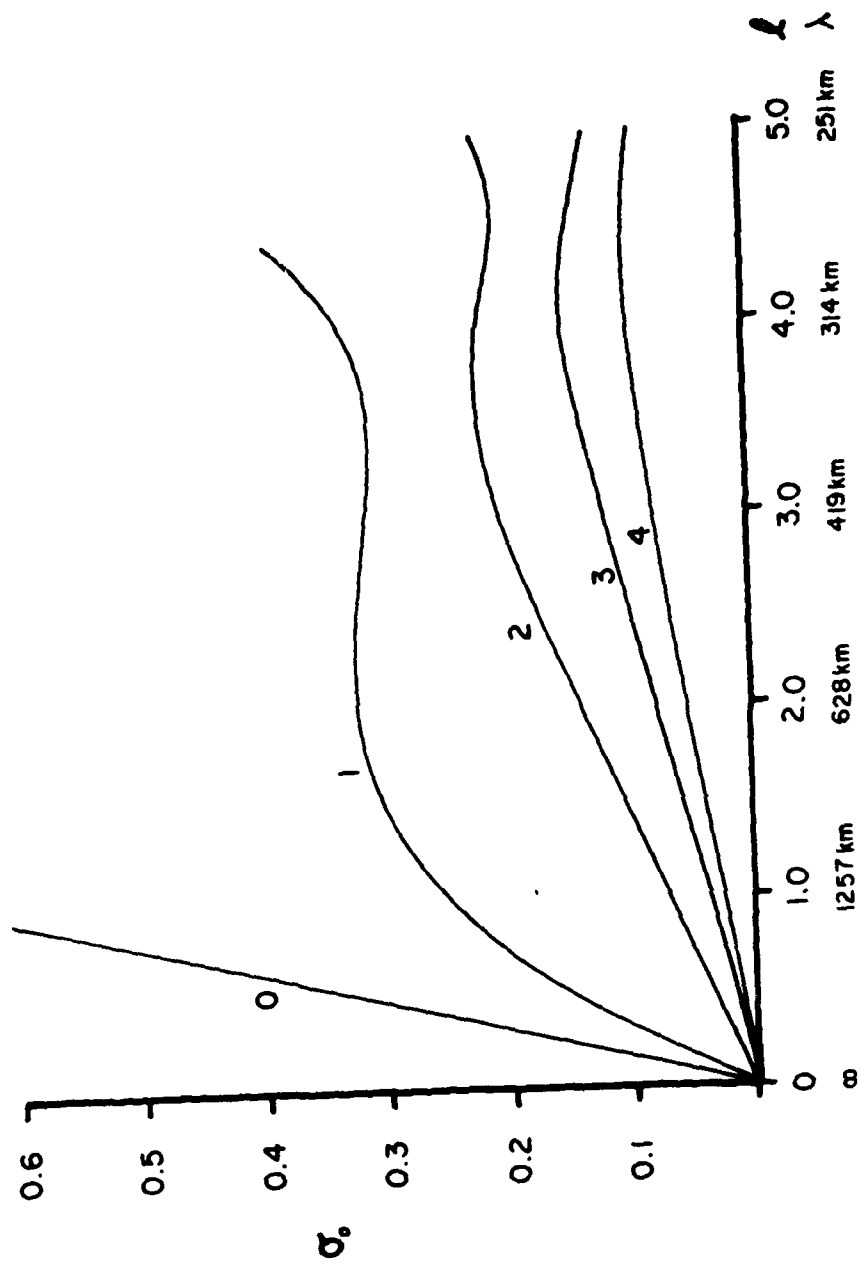


Fig. 5.1

ALONGSHORE VELOCITY V

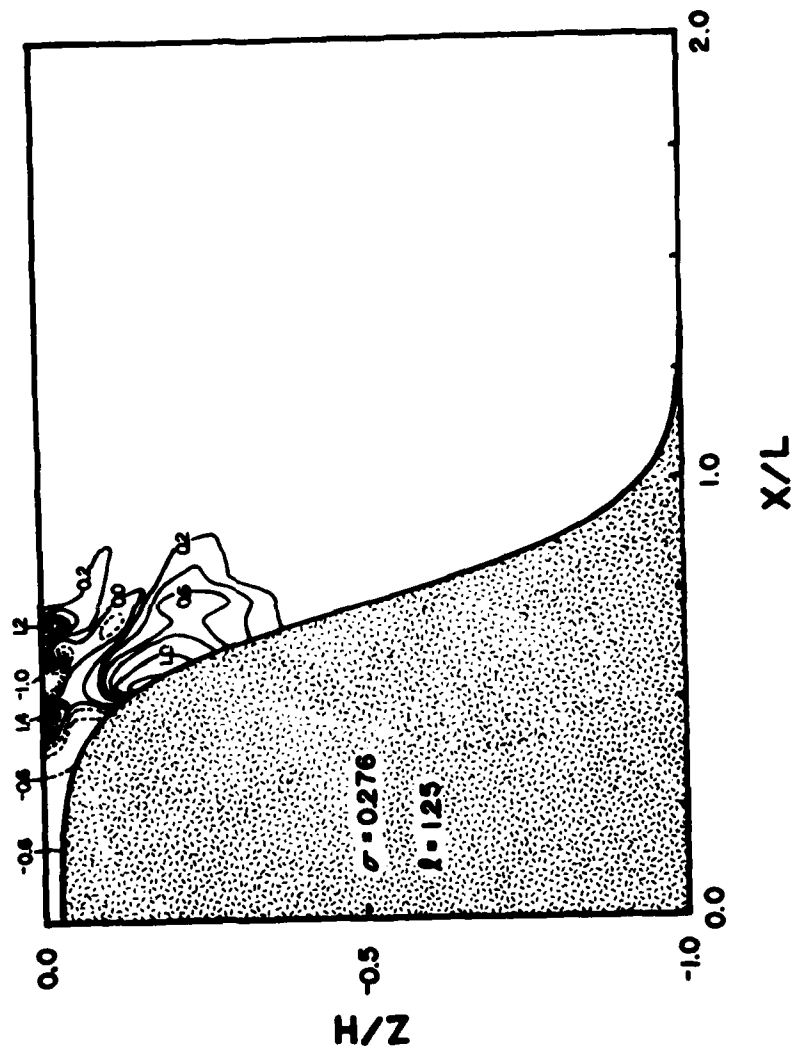


Fig. 5.2(b)

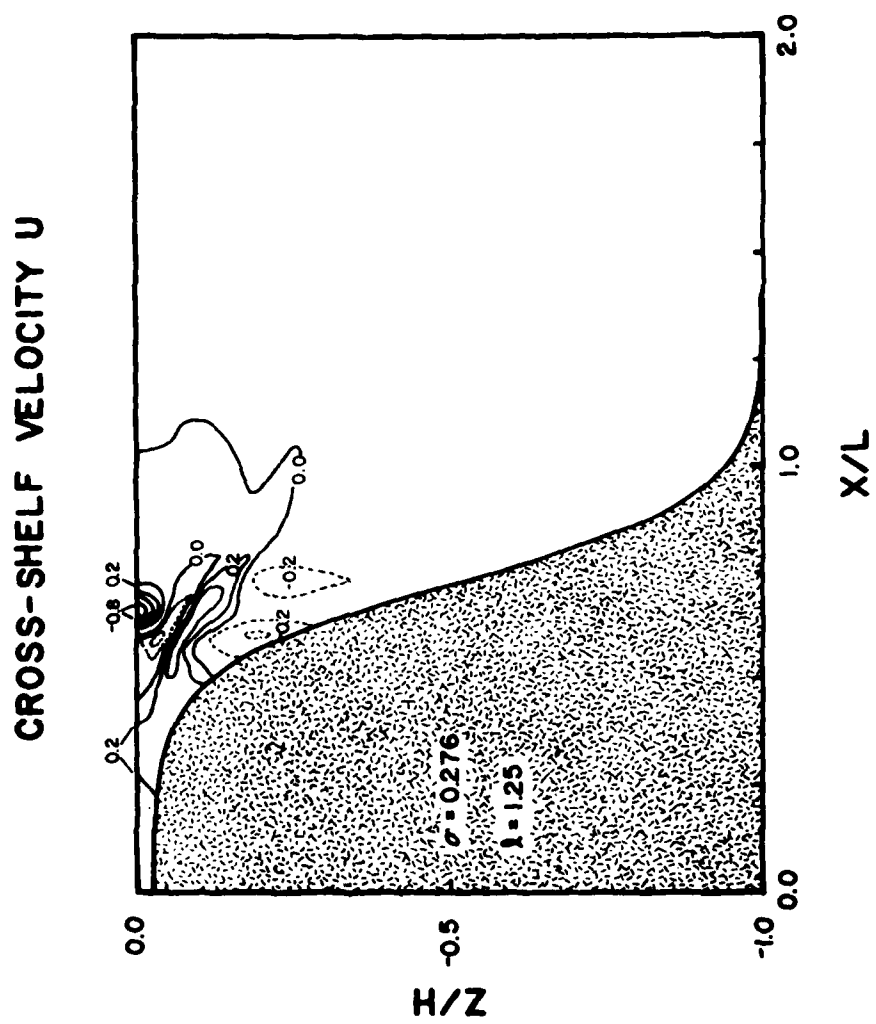


Fig. 5.2(c)

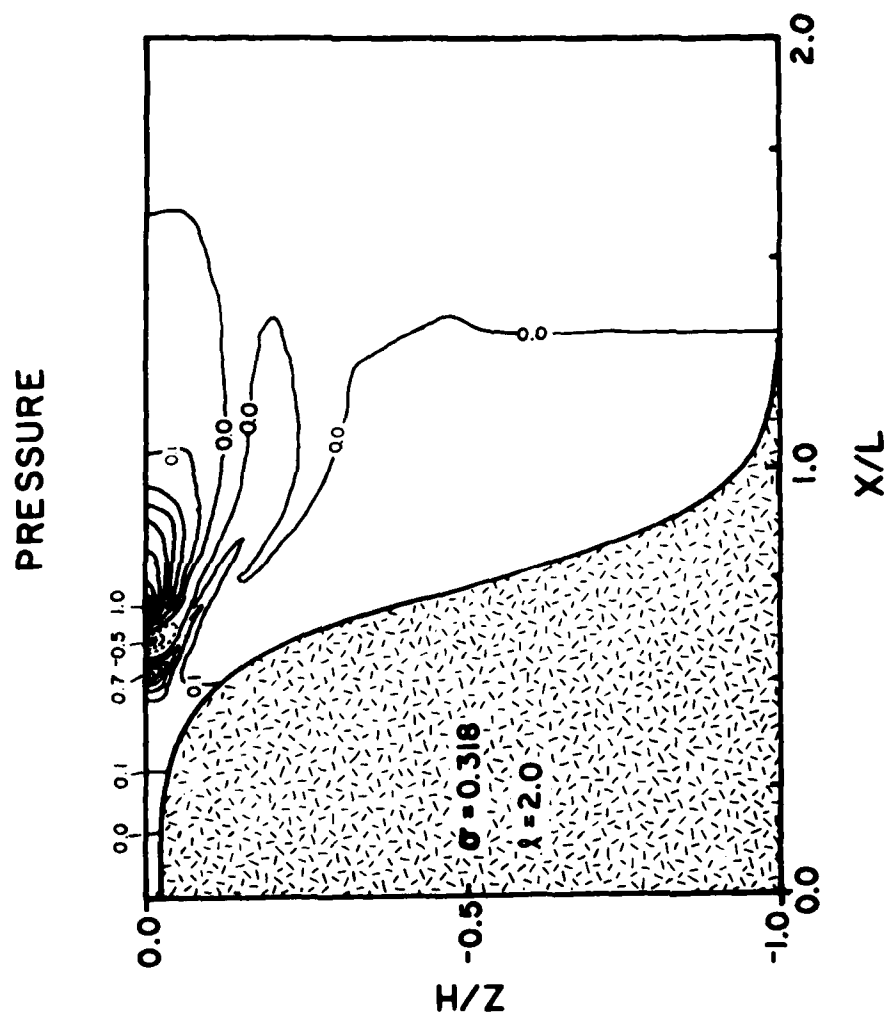


Fig. 5.3

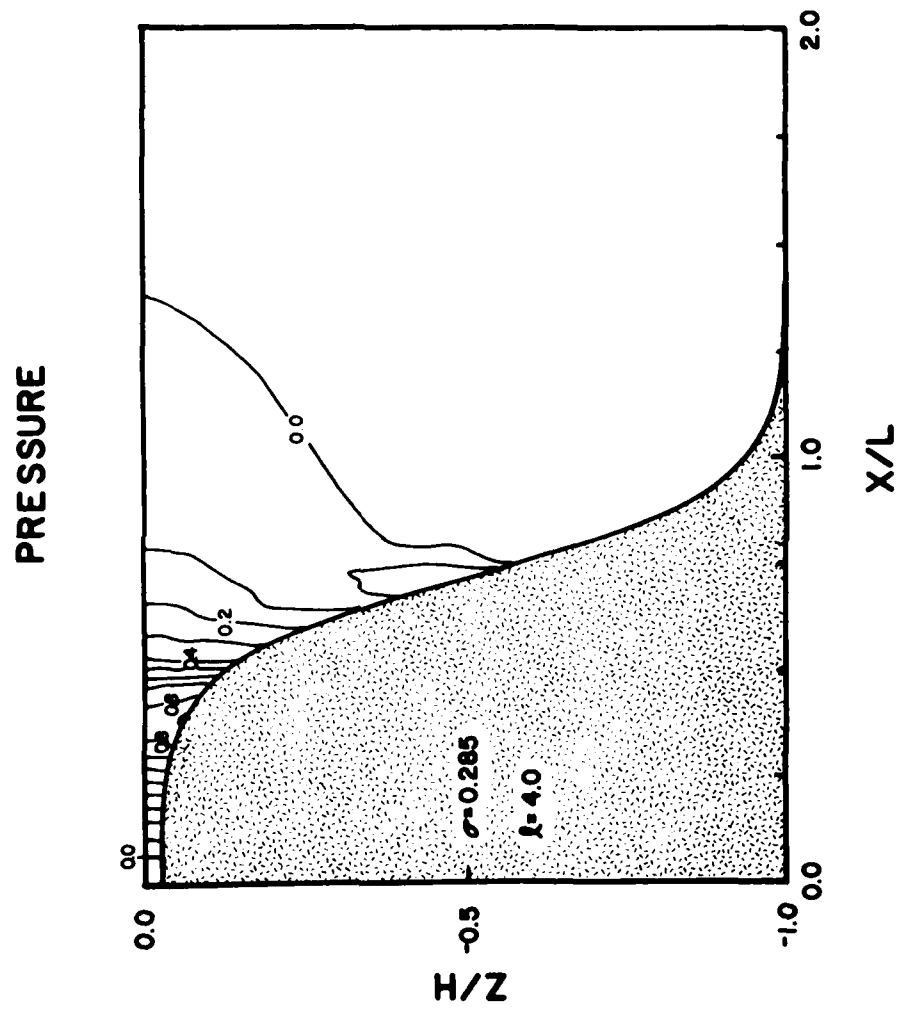


Fig. 5.4

ALONGSHORE VELOCITY V

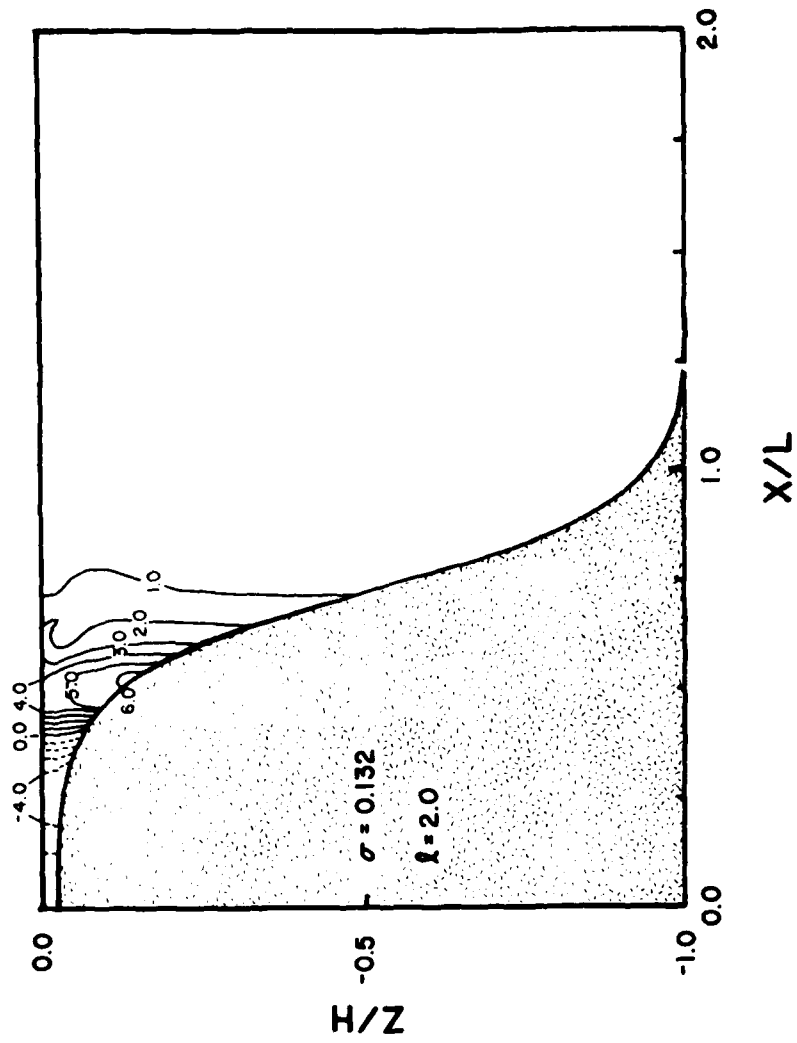


Fig. 5.5(b)

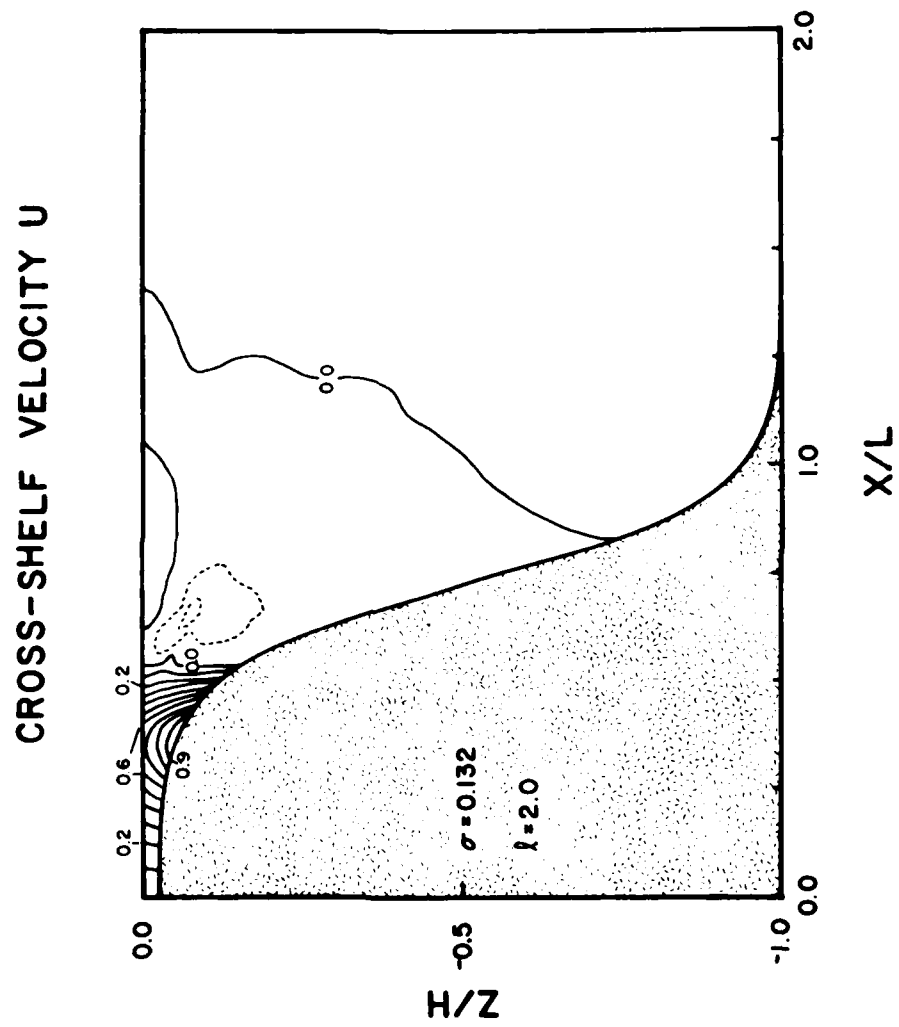


Fig. 5.5(c)

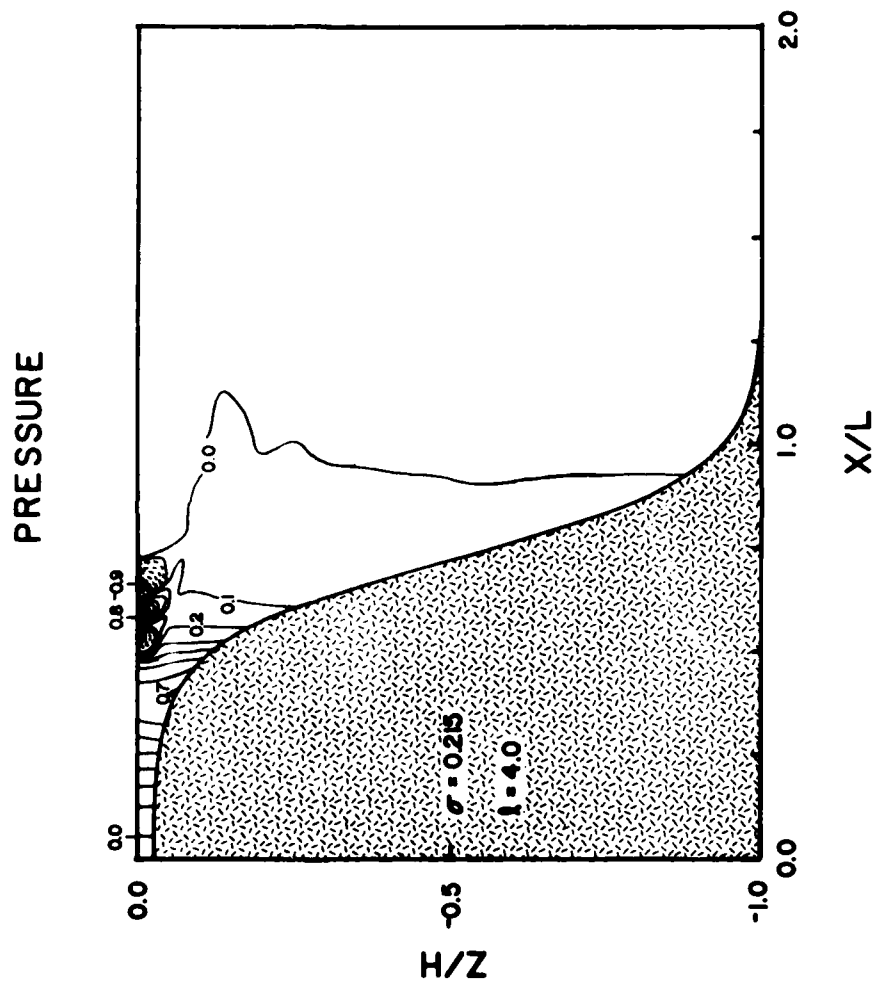


Fig. 5.6

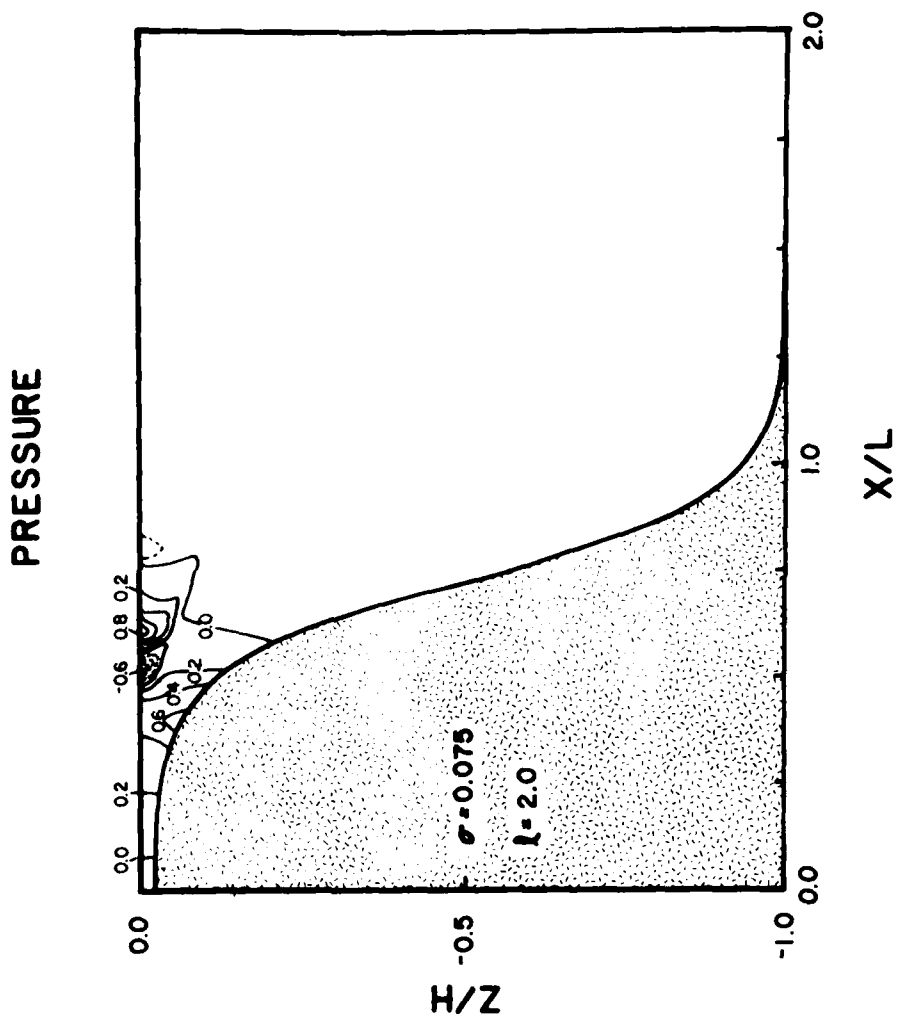


Fig. 5.7

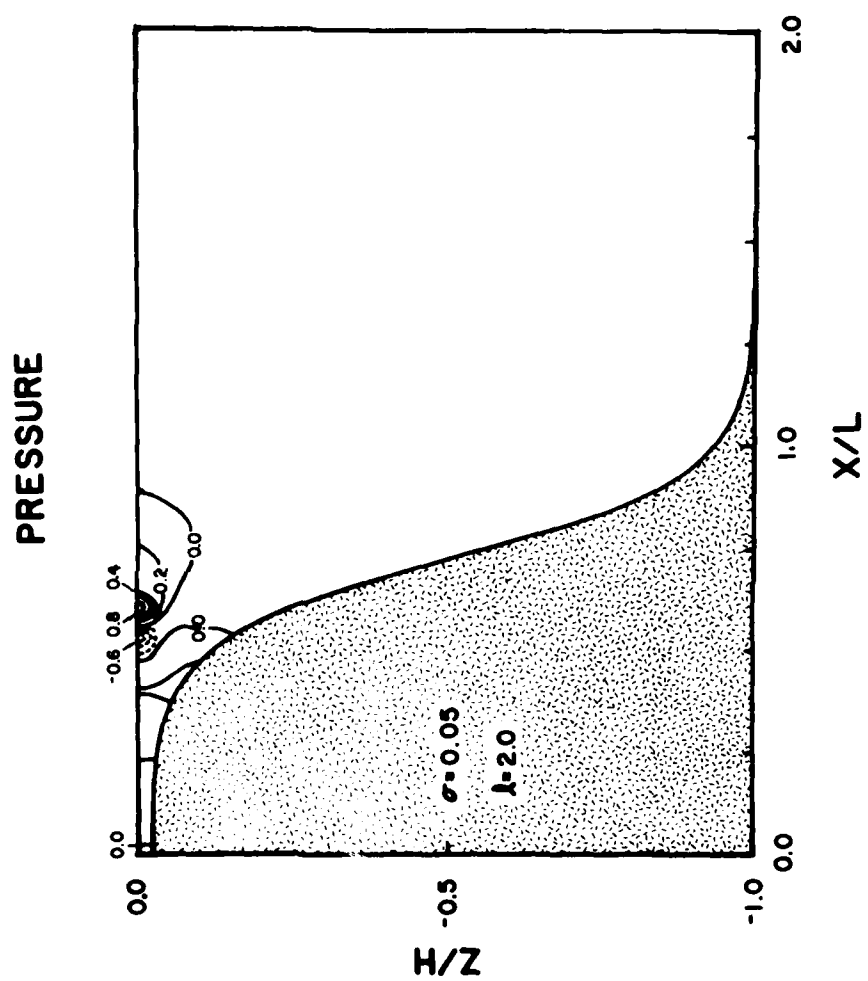


Fig. 5.8

POTENTIAL VORTICITY

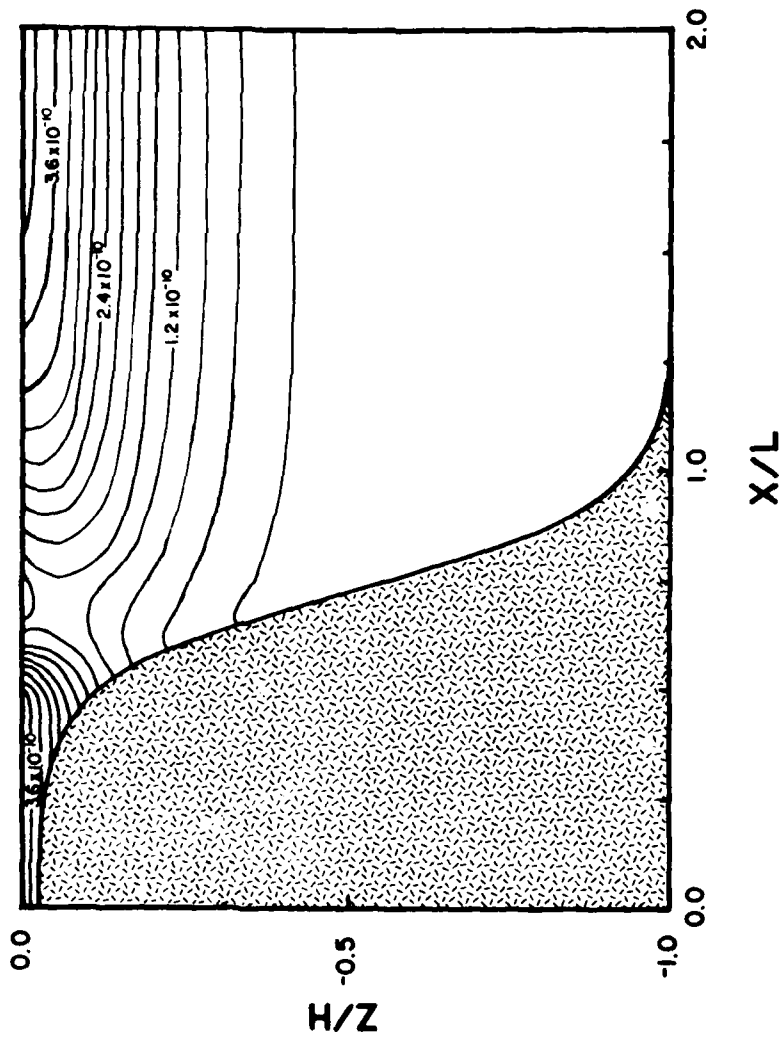


Fig. 5.9

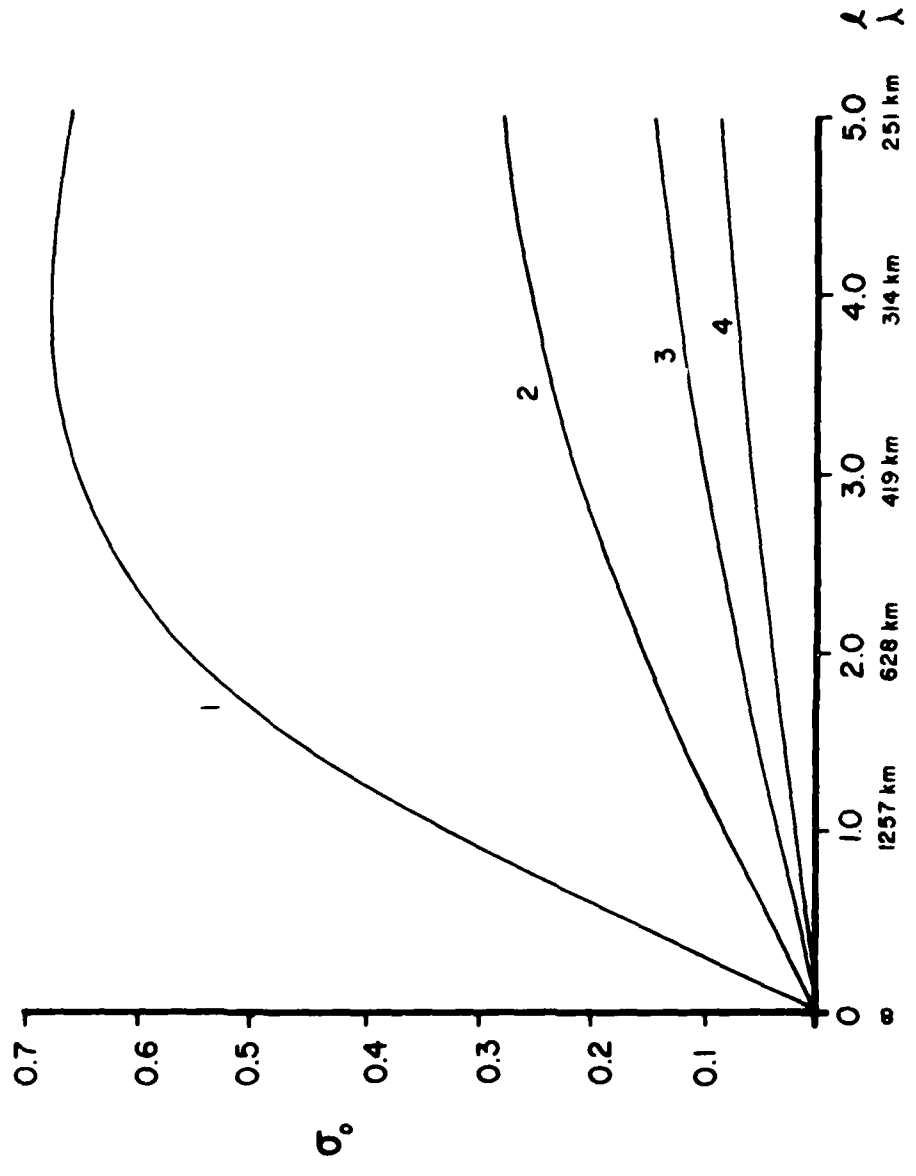


Fig. 6.1

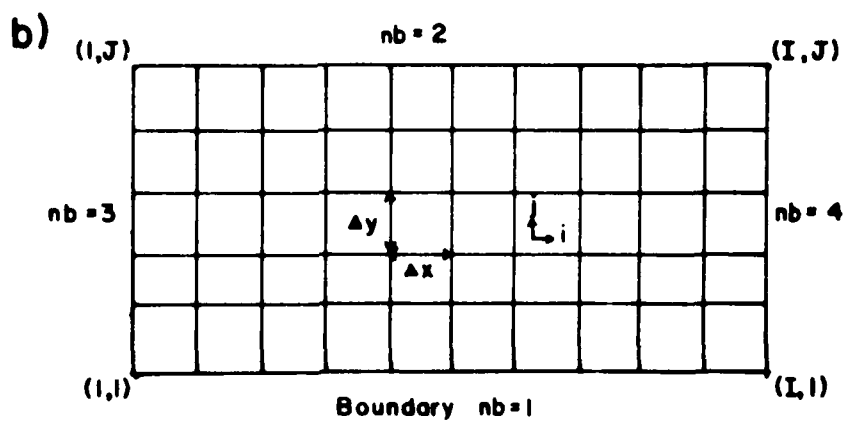
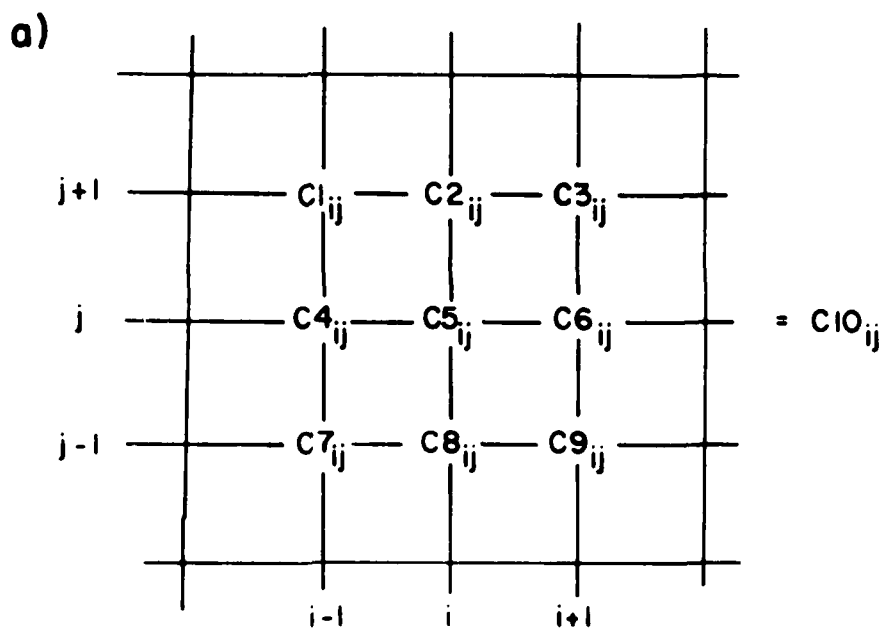


Fig. A3.1